Two-dimensional polaritonic photonic crystals as terahertz uniaxial metamaterials

S. Foteinopoulou,[1,2] M. Kafesaki,[2,3] E. N. Economou,[2,4] and C. M. Soukoulis[2,3,5]

[1]*School of Physics, University of Exeter, Stocker Road, Exeter EX4 4QL, United Kingdom*

[2]*Institute of Electronic Structure and Lasers (IESL), Foundation for Research and Technology-Hellas (FORTH), Heraklion, GR-71110 Crete, Greece*

[3]*Department of Materials Science and Technology, University of Crete, Heraklion, Crete, Greece*

[4]*Department of Physics, University of Crete, Heraklion, Crete, Greece*

[5]*Ames Laboratory-USDOE, and Department of Physics and Astronomy, Iowa State University, Ames, Iowa 50011, USA*

(Received 20 January 2011; published 28 July 2011)

Emerging technologies such as quantum cascade lasers enabled the investigation of the most interesting, yet very little explored, THz part of the electromagnetic (EM) spectrum. These THz sources impose a dire need for novel materials suitable for optical components at such frequencies, as traditional visible optics is not appropriate for THz. Here, we explore two-dimensional (2D) photonic crystals (PCs) with either or both constituents made of polar materials, having a polariton gap within or close to the THz regime. Our objective is to create polaritonic composites that behave as extraordinary effective homogeneous uniaxial media, with flexibly engineered EM wave dispersion and high transmissivity in the THz frequency region. Accordingly, it is most important to be able to identify when 2D composites act as effective bulk uniaxial media. Clearly, deviation from standard effective medium predictions does not necessarily imply bulk effective medium picture breakdown. We developed a reliable criterion which provides a clear angular signature of effective medium behavior in 2D composites, even in the presence of high losses. Relying on this criterion, we characterized polar-dielectric and polar-polar PC composites acting as homogeneous uniaxial metamaterials for any arbitrary incident angle. We selected certain cases of effective metamaterial composites which demonstrate a polarization filter behavior. In particular, our results suggest that an unpolarized source will lead to either an S- or a P-polarized wave just by changing the angle of incidence of the impinging wave, irrespective of the thickness of the composite metamaterial. Furthermore, we show that transmission through a LiF/NaCl composite can be as high as 20%, even though transmission through an identical slab made from either of the two polar constituents would be next to zero. We analyze and discuss the physical origins underpinning such extraordinary angular transmission profile of these metamaterial composites. Our results suggest that appropriate mixing of polar materials with each other or with high-index dielectrics provides a route to making advanced photonic materials that are highly attractive for THz optical components.

DOI: 10.1103/PhysRevB.84.035128 PACS number(s): 81.05.Xj, 78.20.Ci, 41.20.Jb, 42.70.Qs

I. INTRODUCTION

THz EM waves, or otherwise known as T rays, lie between the microwave and IR spectrum with frequencies between 0.1 and 10 THz.[1] Despite their immense technological potential for sensing and tissue imaging, T rays have been very little explored until recently. One of the main obstacles was the scarcity of THz sources, which was overcome by the emerging technology of quantum cascade lasers (QCLs).[2–4] This stresses the need for optical components, as for example polarizing filters and converters, beam diverters and splitters, collimators, and lenses, that are functional at this regime. Nevertheless, standard materials that are used for such components in the visible spectrum do not possess the suitable optical properties to be functional at THz. Accordingly, there is a pressing urge to search for metamaterials which are promising for versatile dispersion engineering of T rays while exhibiting high transmissivity. THz metamaterials with such properties would be highly attractive candidates for optical components at this frequency regime.

Exotic uniaxial effective metamaterials at visible frequencies have been previously reported.[5,6] Such metamaterials are essentially 2D photonic crystal (PC) arrangements of thin metallic wires and were shown to possess superfocusing properties. They owe such extraordinary lensing properties to an unusual shape of the surface of wave normals[7] (or otherwise known as equifrequency surfaces, EFS[8]), which is not possible in any natural material. In particular, they exhibit a hyperbolic EFS emanating from an indefinite effective permittivity tensor,[9] with principal elements of opposite sign. We note that hyperbolic EFS can emanate also from an indefinite effective permeability tensor, typical of magnetic metamaterials.[10] This curious type of EFS introduces allowed propagation directions, despite the existence of a negative permittivity or permeability along certain principal direction(s). At the same time, the open form of the hyperbola in wave vector space cannot impose an upper bound on the permissible parallel component of the wave vector[11,12] and thus supports the transfer of the dark (evanescent) components of the source through the uniaxial metamaterial. In other works, this novel type of engineered EM dispersion facilitates EM propagation inside the effective uniaxial metamaterial even in cases where this would be prohibited in either or both of its respective constituents.

Polar materials also possess a negative permittivity within a certain frequency range known as the polariton gap, which makes them also good candidates for the aforementioned type of uniaxial metamaterials with hyperbolic dispersion. Since for many materials the polariton gap falls within or close to the THz spectrum, polar materials become highly attractive constituents for metamaterials functional at THz. Previously researchers have employed a 2D polar PC with spatial

arrangement chosen so that the polaritonic gap overlaps with the photonic band gap of a corresponding metallodielectric PC.[13] They have found very frequency selective field reconfiguration, which goes from extreme localization to complete field expansion around the polar material within a small frequency window. In this paper, we will study 2D polaritonic PCs that behave as bulk effective homogeneous uniaxial metamaterials for arbitrary illumination and are functional at THz, and thus suitable for optical components at such frequencies.

In particular, by composites acting like bulk uniaxial effective media we mean composites demonstrating a reflective and transmissive behavior that can be entirely described by a permittivity (and/or permeability) tensor with elements that are independent of the thickness of the composite and the angle of incidence of the impinging wave. Standard effective medium descriptions[14–16] that have been extensively used thus far are approximate descriptions. Accordingly, it is of the utmost importance to develop a reliable criterion that ascertains the validity of a homogenized effective medium picture. Clearly, failure of a certain effective medium theory (EMT) to accurately depict the EM response of the system does not necessarily imply that the system cannot be described by an effective medium. The need for a criterion that provides a signature for a bulk effective medium behavior is immense.

This paper is organized as follows: In Sec. II we develop two different criteria, thickness based and angle based, that assert the validity of a bulk effective medium picture for the case of 2D PC composites. We then demonstrate the application of such criteria in a well-studied system—that of a 2D dielectric photonic crystal. We show that both of these criteria arrive at a very reliable identification of the spectral range where the 2D PC medium behaves as a bulk uniaxial effective medium for any arbitrary incident EM wave (on and off the periodic plane). In Sec. III we test the transferability of such criteria to polaritonic composite structures. We find that only the angle-based criterion is appropriate and generalize its form to encompass 2D composites with lossy and resonant constituents. We use such criterion to characterize effective medium behavior of candidate polaritonic-dielectric and polaritonic-polaritonic structures. Subsequently, we investigate the transmission properties of selected composites in Sec. IV. We analyze and explain their extraordinary angular transmission profile, which can make them suitable optical components, in Sec. V. Finally, we present our conclusions in Sec. VI.

II. EFFECTIVE MEDIUM BEHAVIOR SIGNATURE IN 2D PERIODIC COMPOSITES

Effective medium pictures for heterogeneous composites have been developed since the beginning of the 20th century,[14,15] with more recent research[16] targeting the specific case of two-dimensional (2D) photonic crystals (PCs) of cylindrical rods. In particular, it was found that at the long-wavelength limit a 2D PC with rods of dielectric constant ε_1 that are embedded in a host material (matrix) with dielectric ε_2 behaves as an effective medium with distinctly different permittivity for propagation with electric field parallel to the rods (E waves) [see Fig. 1(a)], and for propagation with magnetic field parallel to the rods (H waves) [see Fig. 1(b)]. In other words the expected effective permittivity for E waves, ε^E, would be

$$\varepsilon^E = f_r\varepsilon_1 + (1 - f_r)\varepsilon_2, \tag{1}$$

while the expected effective permittivity for H waves, ε^H, would be

$$\varepsilon^H = \varepsilon_2 \frac{(1 + f_r)\varepsilon_1 + (1 - f_r)\varepsilon_2}{(1 - f_r)\varepsilon_1 + (1 + f_r)\varepsilon_2}, \tag{2}$$

with f_r representing the fraction covered by the rod cross section on the periodic plane, known as filling ratio. We recognize in Eq. (2) the Maxwell-Garnett result,[15] which applies to cermet topologies, as is the case of a nonoverlapping PC.

There have been a number of works that attempt to go beyond the simple effective medium formulas shown above, and extend the frequency range of the description of the system as a homogenized medium.[17–22] However, the dire question that remains is the following: Are there any identifiable signature behaviors for an effective medium behavior of a heterogeneous composite structure? Evidently, mismatch between actual transmission or reflection and the one predicted from a homogenized model does not necessarily imply failure of effective medium picture. It would be of particular interest to be able to identify a signature for a bulk effective medium behavior of a certain composite by properly analyzing its transmissive or reflective behavior. In the following, we proceed to develop criteria establishing such signature of bulk effective medium picture.

Let us consider a composite material slab composed of a sufficient number of meta-atom building blocks. If such composite behaves as a bulk effective metamaterial, then its optical properties should be independent both of its thickness and of the angle of incidence. Since the optical response is distinctively different for E waves and H waves, it is expected that the optical response of a 2D periodic composite metamaterial would be described with a permittivity tensor given by

$$\bar{\bar{\varepsilon}} = \begin{bmatrix} \varepsilon^H & 0 & 0 \\ 0 & \varepsilon^E & 0 \\ 0 & 0 & \varepsilon^H \end{bmatrix}. \tag{3}$$

If in addition an effective magnetic behavior is present, then the optical constitutive parameters would also include a permeability tensor given by

$$\bar{\bar{\mu}} = \begin{bmatrix} \mu^E & 0 & 0 \\ 0 & \mu^H & 0 \\ 0 & 0 & \mu^E \end{bmatrix}. \tag{4}$$

In the above expressions, we assumed that the rods of the 2D composite are aligned along the y axis, which is also the optical axis of the uniaxial metamaterial, and arranged periodically on the xz periodic plane (as seen in Fig. 1). The E and H superscripts in the elements of the permittivity and permeability tensors correspond to the constitutive parameters under E-wave and H-wave incidence, respectively. In Appendix A, we recap the expected transmission T and reflection R, as well as the reflectivity over transmissivity ratio r/t for a general homogeneous uniaxial medium of thickness

L, constitutive parameters given by Eqs. (3) and (4), and under the illumination conditions depicted in Fig. 1.

For a thickness-based test of effective medium validity we assume normal incidence; i.e., $\theta_I = 0$. If the composite does behave like an effective medium, then the complex reflectivity r and transmissivity t must satisfy Eq. (A3) for any arbitrary thickness L, with χ given by Eq. (A7). Let us define a parameter η given by

$$\eta \equiv \frac{1}{\chi - 1/\chi}. \tag{5}$$

Evidently, such parameter should be independent of L. After application of Eq. (A3) for two different thicknesses, L and $2L$ respectively, it is easy to show after some math manipulation

$$|\mathrm{Re}(\eta)| = \left| \mathrm{Re}\left[i \frac{\sin\left[\cos^{-1}\frac{\left(\frac{r}{t}\right)_{2L}}{2\left(\frac{r}{t}\right)_L}\right]}{2\left(\frac{r}{t}\right)_L} \right] \right| \tag{6}$$

and

$$|\mathrm{Im}(\eta)| = \left| \mathrm{Im}\left[i \frac{\sin\left[\cos^{-1}\frac{\left(\frac{r}{t}\right)_{2L}}{2\left(\frac{r}{t}\right)_L}\right]}{2\left(\frac{r}{t}\right)_L} \right] \right|. \tag{7}$$

Note that $\cos^{-1}$ in the above equations represents the principal value of the function. Equations (6) and (7) imply that for a composite material that behaves as an effective medium the actual calculated values of the right-hand side must be more or less constant. Put differently, Eqs. (6) and (7) provide the means to quantify the applicability of the effective medium picture for a certain system, by calculating the variance of the quantities $|\mathrm{Re}(\eta)|$ and $|\mathrm{Im}(\eta)|$, with different values of the sample thickness L. The larger the magnitude of such variance the larger the deviation from the effective medium picture. Also, for particular cases with only inherently lossless constituents, the right-hand side of Eq. (7) should yield zero. The mere appearance of a significant imaginary part in η would signify the breakdown of effective medium behavior.

In order to evaluate the thickness criterion developed above, we test it on a well-studied system. In particular, we will investigate a two-dimensional photonic crystal composed of Si rods in a square lattice arrangement embedded in air, under illumination conditions shown in Fig. 1 and normal incidence. As drawn in Fig. 1 both the interface and propagation direction z lie along the ΓX symmetry direction. We take the dielectric constant of Si to be equal to 11.56 and diameter of the rods to be $0.6a$, with a being the lattice constant of the square lattice, corresponding to a filling ratio $f_r = 0.2827$. For this type of dielectric PC, which has frequency scalable properties,[24,25] we will quote frequency f in dimensionless units, fa/c, with c being the velocity of light.

We proceed now to apply the thickness test for such structure. For this purpose, we calculate with the transfer matrix method (TMM),[26] the ratio of the complex reflection and transmission amplitudes r/t, for different thicknesses L. In particular, we vary L from $1a$, to $30a$ with a step of $1a$ and from $30a$ to $60a$ with a step of $2a$. In this manner, we are able to construct numerically the absolute value of the real

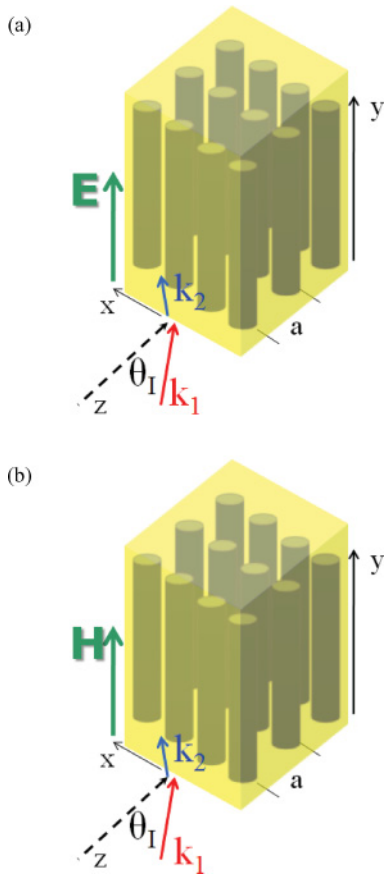

FIG. 1. (Color online) EM waves incident from vacuum, with an angle θ_I, into a uniaxial anisotropic medium corresponding to a homogenized 2D PC composite. $\mathbf{k_1}$, and $\mathbf{k_2}$ represent the wave vectors in vacuum and inside the homogenized uniaxial medium, respectively. In (a) we see a case with the electric field perpendicular to the plane of incidence xz (E polarization or E waves). Conversely in (b) we see a case with the magnetic field perpendicular to the plane of incidence xz (H polarization or H waves) (Ref. 23).

and imaginary parts of η with the use of Eqs. (6) and (7), for values of L ranging from $1a$ to $30a$ with a step of $1a$. From these we are able to obtain the average values of $|\mathrm{Re}(\eta)|$ and $|\mathrm{Im}(\eta)|$ over many thicknesses, and associated variances as a function of the dimensionless frequency fa/c.[27–29] We have included in these quantities data with $L \geqslant 2a$, as we always observe an abrupt change in $|\mathrm{Re}(\eta)|$ and $|\mathrm{Im}(\eta)|$ from $L = 1a$ to $L = 2a$, implying that we do not have bulk properties for a single layer of cylinders.

We plot the average values of $|\mathrm{Re}(\eta)|$ and $|\mathrm{Im}(\eta)|$, $\overline{|\mathrm{Re}(\eta)|}$ and $\overline{|\mathrm{Im}(\eta)|}$, respectively, in Figs. 2(a) [3(a)] and 2(c) [3(c)] for the case of E waves (H waves) versus the dimensionless frequency fa/c. The corresponding variances are shown in Figs. 2(b) and 2(d) [3(b) and 3(d)] for the case of E waves (H waves). Note that the PC band gap regions along ΓX for E waves are shown in Fig. 2 as lightly shaded regions. There are no band gaps along ΓX for H waves, but we indicate the band edge at the X symmetry point where the first and second bands anticross with the vertical dotted lines in Fig. 3. The dark-shaded region represents a frequency region where

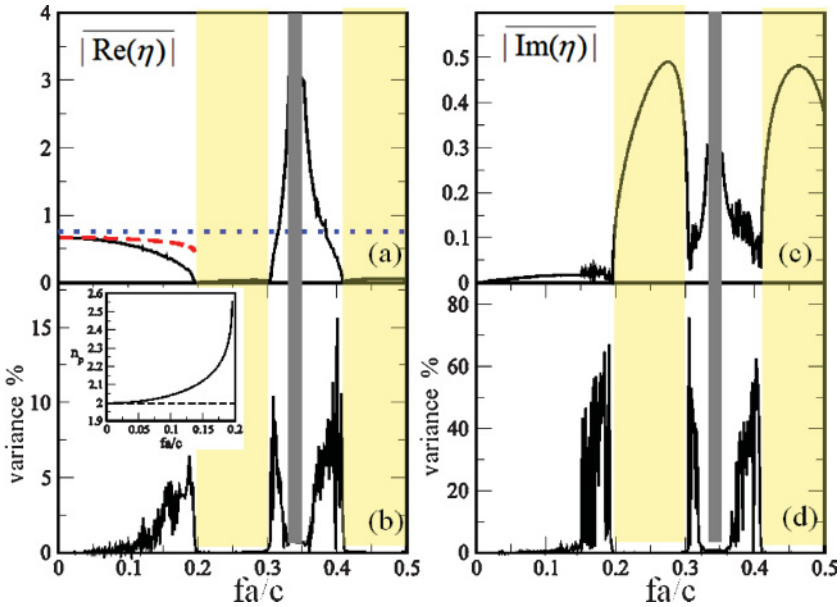

FIG. 2. (Color online) Quantifying validity of effective medium picture with the thickness test in a 2D dielectric PC structure for E waves [incident as shown in Fig. 1(a) for $\theta_I = 0$]. The absolute values of the real and imaginary part of η are calculated numerically for different thicknesses L (Refs. 27–29). The corresponding averages are shown in panels (a) and (c), respectively, with the respective variances shown directly below [panels (b) and (d)]. The prediction for the η parameter from EMT [Eq. (1)] is shown as the dotted line in (a). The dashed line represent the value corresponding to a refractive index n_p extracted from the band structure along ΓX direction [shown in the inset of panel (b)]. The light-shaded region represent band gap regions, while the dark-shaded region is a region were no data could be obtained (Ref. 27–29).

it was not possible to have data due to low $|r/t|$ values for many thicknesses.[27–29] The dotted horizontal line in Figs. 2(a) and 3(a) represents the $|\mathrm{Re}(\eta)|$ calculated with the use of the effective medium dielectric constant [Eq. (1) and Eq. (2), respectively]. We also extract a refractive index n_p from the band structure[25] along ΓX,[8] i.e., $n_p = ck/\omega$, with k being the wave vector along ΓX. Incidentally, we note that a retrieved refractive index from r/t given from Eq. (D3), following the procedure detailed in Appendix D, is in excellent agreement with the band structure extracted index. We show the latter in the inset of Fig. 2(a) [3(a)] for the case of E waves [H waves]. We have calculated a $|\mathrm{Re}(\eta)|$ value corresponding to this index and depict this as a dashed line in Figs. 2(a) and 3(a). Note that field averaging, Maxwell-Garnett EMTs, and band structure based homogenization would predict a zero value for $|\mathrm{Im}(\eta)|$.

For both E waves and H waves we observe that the band structure and numerically extracted $|\mathrm{Re}(\eta)|$ value agree well for frequencies where the variance is low. As the variance increases also the disagreement between the two increases. This coincides with the appearance of an increasing imaginary part in η—which is also characterized by very high variance—signifying the breakdown of the effective medium picture. What is surprising is that when we are inside band gaps, there is a large extracted imaginary part of η, but nevertheless the variance of $|\mathrm{Im}(\eta)|$ is low. We could argue that the system can be described perhaps in such cases by an artificial effective medium. We will discuss this point further later in this section.

As a confirmation of the reliable prediction of effective medium validity through the thickness test, we compare the transmission versus thickness L between the actual PC and a suitable homogeneous medium for both E waves

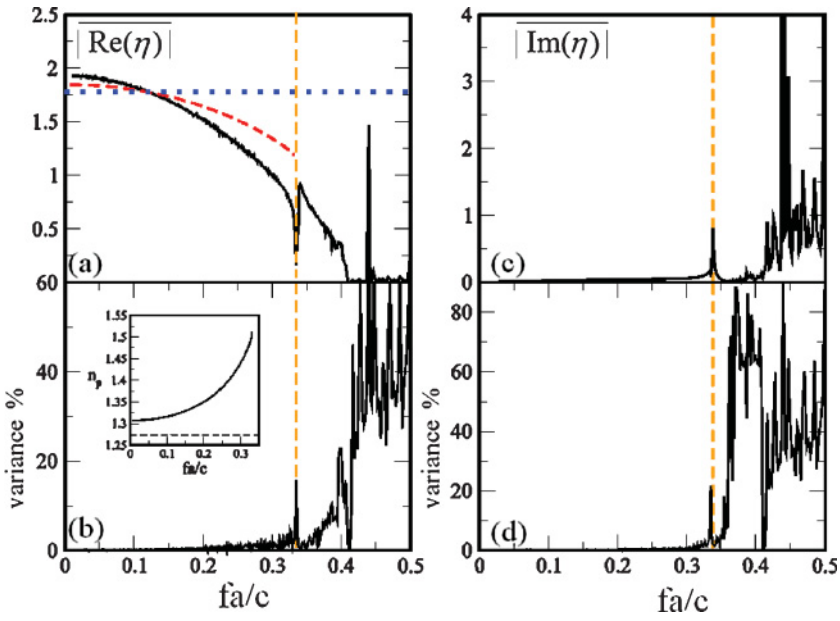

FIG. 3. (Color online) Same as in Fig. 2 but for the case of H waves [incidence as shown in Fig. 1(b) for $\theta_I = 0$]. Here, we do not have any band gap in the plotted region along the propagation direction (ΓX). The vertical dashed lines (not present in Fig. 2) represent the frequency where the first and second band of the H waves anticross at the X symmetry point.

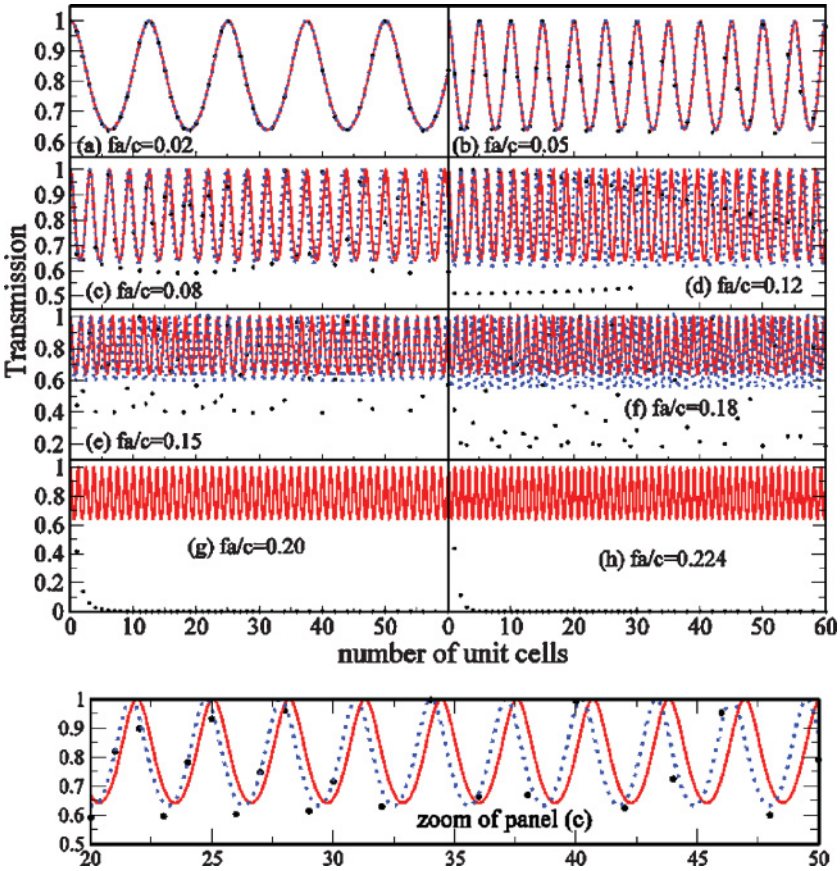

FIG. 4. (Color online) E-wave transmission results vs PC thickness, for various frequencies, designated in each panel in dimensionless units fa/c, with a being the lattice constant and c the velocity of light. We compare transmission between the actual PC medium (filled circles), a homogenized medium with permittivity corresponding to the field-averaging effective permittivity [Eq. (1)] (solid lines), and a homogenized medium with refractive index n_p extracted from the band structure [inset of Fig. 2(b)] (dotted line). The transmission results corresponding to band structure extracted index are not shown for the cases of panels (g) and (h) because the respective frequencies lie beyond the first band edge. We have zoomed inside panel (c) and show this in the bottom panel. This highlights the excellent agreement between actual PC transmission and the transmission corresponding to a homogenized medium with refractive index n_p. Note the apparent discrepancy for this case with a homogenized medium with permittivity corresponding to the field-averaging formula of Eq. (1).

and H waves at normal incidence. The transmission for the actual PC structure is calculated with the TMM method,[26] while we use the formulas in Appendix A to calculate the transmission of the homogenized PC. We assume two different types of homogenized media. For the first type we assume optical parameters which correspond to field averaging for the case of E waves [Eq. (1)] and Maxwell-Garnett theory for the case H waves [Eq. (2)]. For the second type, we assume the band structure extracted refracted index, shown in the insets of Figs. 2(b) and 3(b) for E waves and H waves, respectively.

We plot the results in Figs. 4 and 5, respectively, for various dimensionless frequencies, fa/c, which are designated inside the corresponding subfigures. The TMM results are indicated with the filled solid circles. The effective medium results according to Eqs. (1) and (2) are shown as solid lines, while the results corresponding to the second type of effective medium with parameters extracted from the band structure are plotted as dotted lines. The effective medium description from Eqs. (1) and (2) does not seem to cover the full frequency range of effective medium picture validity as predicted by the thickness test. On the other hand, we find most excellent agreement between actual transmission and transmission of the second type of homogenized medium up to dimensionless frequencies of $fa/c = 0.08$ for E waves and $fa/c = 0.15$ for H waves. We can see this clearly in the bottom panels of Figs. 4 and 5 which are a zoomed version of panels Fig. 4(c) and 5(c), respectively. These results suggest that indeed the thickness test is a rigid indicator for the suitability of an effective medium picture for the dielectric PC.

Despite the clear reliability of the thickness test developed above, there are certain shortcomings. An obvious one is the requirement to obtain r/t for a large number of thicknesses, which makes it overly tedious. However, the main disadvantage of the thickness test is that it cannot be applied to lossy media, which is the case of polaritonic composites. This is because as absorption increases with thickness, t becomes negligible. We therefore are in need of a test that does not require very large thicknesses, so that it would be transferable in lossy media composites, which is the case of our interest in this paper.

We will construct a second test probing the angular response of r/t for the actual structure, with incident angles θ_I as seen in Fig. 1. If the effective medium picture is valid the angular response of the system should also be close to that corresponding to a homogeneous medium. After some math manipulation we obtain from Eq. (A3)

$$\sin^2\theta_I = \frac{c^2}{\omega^2 L^2}\left[B(\theta_I = 0) - B(\theta_I)\right] \equiv A(\theta_I) \qquad (8)$$

for the case of E waves and H waves.

The quantity B in expressions (8) is

$$B(\theta_I) = \mathrm{Re}\left(\cos^{-1}\frac{\left(\frac{r}{t}\right)_{2L}}{2\left(\frac{r}{t}\right)_L} + \; l\pi\right)^2_{\theta_I}, \qquad (9)$$

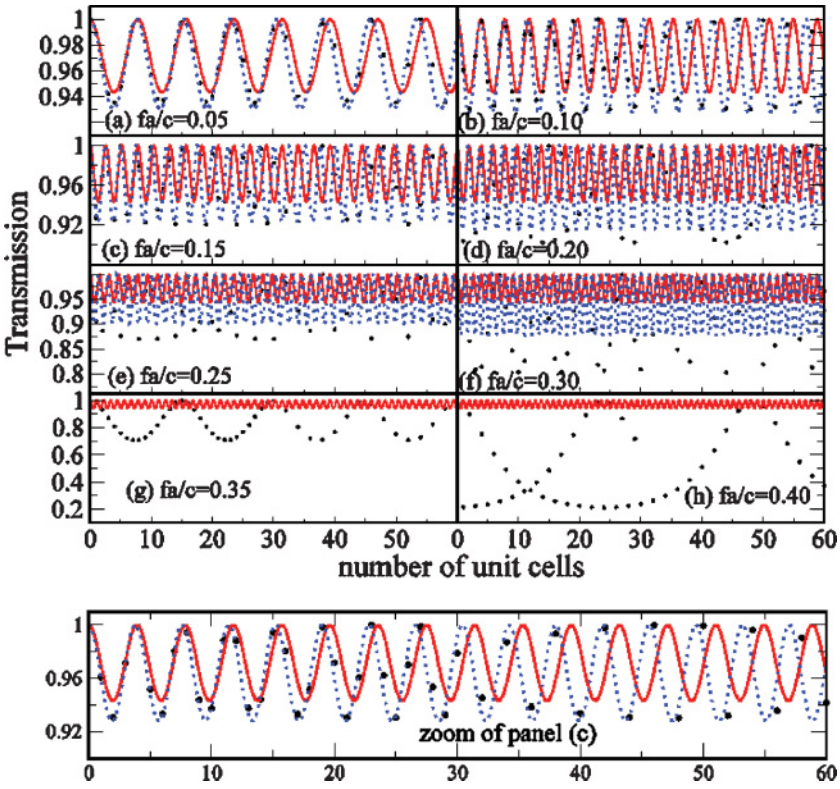

FIG. 5. (Color online) Same as in Fig. 4 but for the case of H waves, with the bold lines representing transmission corresponding to the Maxwell-Garnett permittivity, expressed in Eq. (2). The extracted band structure index n_p used for the transmission spectra given with the dotted lines is given in the inset of Fig. 3(b).

with $\cos^{-1}$ representing the principal value of the function and the integer l representing the choice of the branch. Accordingly, if the system behaves as a homogeneous medium, one of the branches of $A(\theta_I)$ defined in Eq. (8) will be common for different thicknesses L. This common branch should additionally show a $\sin^2$ functional dependence with the angle of incidence θ_I for both E waves and H waves. In other words, the $\sin^2$ functional form of $A(\theta_I)$ constitutes a signature for a behavior of the composite as a bulk uniaxial effective metamaterial. In the following, we call the search for such signature the "angle test."

We first apply the angle test for E waves for the same PC system we investigated with the thickness test for E waves, i.e., under illumination shown in Fig. 1(a). We do so for PC thicknesses of L and $2L$, for different incident angles θ_I ranging from 0° to 90°. We construct the right-hand side of Eq. (8) from the r/t values calculated from the TMM method.[26] We show in Fig. 6 the different branches of $A(\theta_I)$ for different values of thickness L. The circles, diamonds, and x's represent thicknesses $L = 5a$, $L = 7a$, and $L = 10a$, respectively, where a is the lattice constant shown in Fig. 1. Unavoidably, in some cases a range of angles may be missing from our analysis, as we do not include points with low r/t values.[27]

In panels (a), (b), and (c) of Fig. 6 we show the results for dimensionless frequencies fa/c equal to 0.02, 0.10, and 0.224, respectively. For frequency $fa/c = 0.02$ we observe the existence of a common branch that follows excellently a $\sin^2\theta_I$ function, shown as the dashed line for comparison. We see the corresponding result in Fig. 6(a). The inset in Fig. 6(a) is a blowup of the middle part of the figure to emphasize such excellent agreement. For frequency $fa/c = 0.10$ [Fig. 6(b)] we observe the existence of branch solutions for $L = 5a$, $7a$, and $10a$ that lie quite close to each other and close to the dashed line representing the $\sin^2\theta_I$ function, but with some identifiable disagreement. The latter increases for larger frequencies. So the angle test implies that the effective medium picture for E waves starts to break down approximately at $fa/c = 0.10$. Such conclusion is in line with the analysis from the "thickness test." Our observations for H waves are similar, which put the effective medium break down point at about $fa/c = 0.13$.

It is interesting to check what happens in the band gap, where surprisingly we find a small variance on $|\mathrm{Re}(\eta)|$ and $|\mathrm{Im}(\eta)|$ with the thickness test. We show in Fig. 6(c) the angle test result for a frequency lying well inside the band gap ($fa/c = 0.224$). Surprisingly we find a common branch solution for $L = 5a$, $7a$, $10a$ in such a case and we point this out in the figure with the small black arrow. However, this solution does not follow at all the characteristic $\sin^2\theta_I$ dependence. This result, together with the existence of a high imaginary part in η, suggests that we may be able to describe the PC in such a case as an effective medium. However, the effective medium in this case is just as an artificial parametrization.

From the above we can conclude that the angle test is sufficient to determine effective medium validity. Because we can choose smaller thicknesses to apply it, it is transferable to cases involving lossy components. So, to characterize effective medium behavior of the polaritonic composites we will rely on the $\sin^2$ characteristic signature of the angle test. Our ultimate goal is to construct polaritonic composites that behave as uniaxial metamaterials for any arbitrary angle of incidence. It is so essential to investigate the effective response of the medium as a whole, irrespective of the illumination conditions. Accordingly, we should understand how to transfer knowledge for effective medium validity frequency ranges for E waves

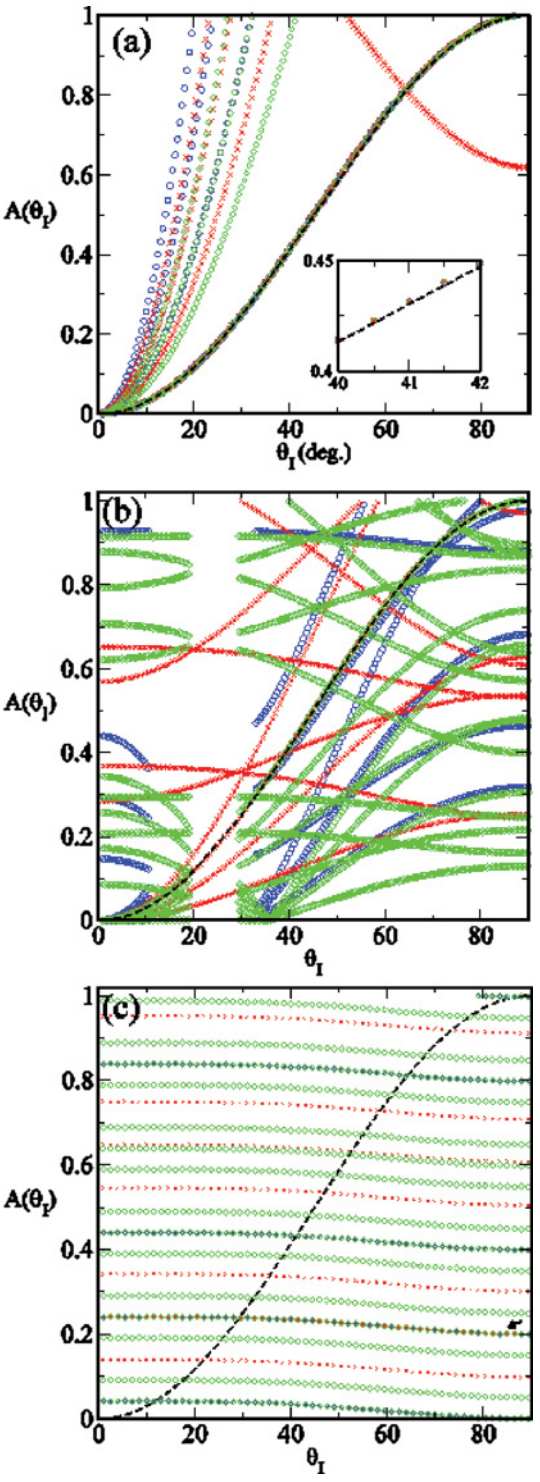

FIG. 6. (Color online) The angle test for E waves on a square dielectric PC (same parameters as the PCs considered in Figs. 2–5). The horizontal axis represents the incident angle θ_I, and the vertical axis represents the quantity $A(\theta_I)$ which is defined in Eq. (8). The circles, x's, and diamonds are for PC thickness values $L = 5a$, $7a$, and $10a$, respectively, with a being the lattice constant. The continuous dashed line represents the $\sin^2$ function. Panels (a), (b), and (c) respectively represent the results for different dimensionless frequencies fa/c with c the velocity of light. In particular $fa/c = 0.02$, 0.10, and 0.224 in (a), (b), and (c), respectively.

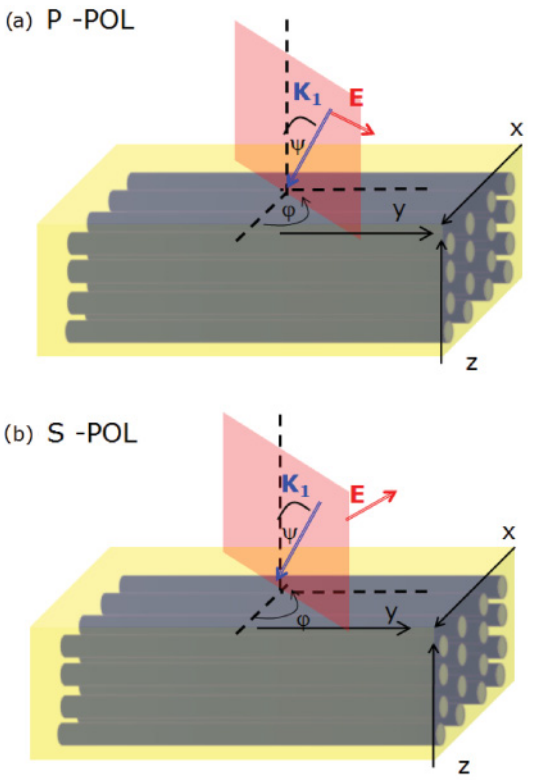

FIG. 7. (Color online) Incidence out of the periodic plane on a 2D square photonic crystal, seen as rods in the figure. The embedding box represents the equivalent homogenized uniaxial medium. We show the P-polarization case in (a) and the S-polarization case in (b). ψ indicates the angle between the surface normal and the incident wave vector $\mathbf{k_1}$. The azimuth angle ϕ represents the angle between the plane of incidence (shaded parallelepiped) and the x direction. The latter represents the periodic direction along the surface. Special cases with $\phi = 0$ or $\phi = \pi$ represent conventional incidence in the periodic plane, leading to H waves for the P-polarization case and to E waves for the S-polarization case, as seen in Fig. 1.

and H waves, respectively, as obtained from the angle test, to cases of arbitrary incidence. We show the square PC, along with the homogenized slab, in Fig. 7, where we depict P- and S-polarized waves incident at an arbitrary direction characterized by the angles ψ and ϕ, also designated in the figure. (For incidence out of the periodic PC plane, we cease to have E and H waves.[30])

The propagation inside a general uniaxial medium under arbitrary illumination is quite complex involving in general the simultaneous propagation of two different beams, corresponding to different surfaces of wave normals[31] (also known as equifrequency surfaces, EFS[8,32]). One is known as the extraordinary beam, and the other as the ordinary beam. We depict a general case in Fig. 8. Note that specific illumination conditions yield single-beam propagation. These are the cases with azimuth $\phi = 0$, π, which will yield E waves or H waves. Also, cases with $\phi = \pi/2, 3\pi/2$ yield single-beam propagation, which is extraordinary if the P-polarized wave is incident, or ordinary if the S-polarized wave is incident. For consistency and completeness we recap the dispersion relations $\omega(\mathbf{k})$, yielding the surfaces of wave

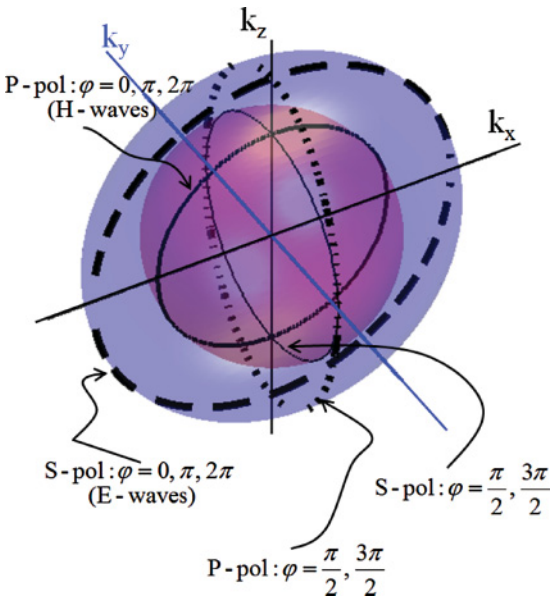

FIG. 8. (Color online) The surfaces of wave normals, for a uniaxial slab with optical axis along y. The outer (inner) ellipse (sphere) represents the dispersion relation $\omega(\mathbf{k})$ for the extraordinary (ordinary) mode. For waves incident at arbitrary azimuth, coupling to both extraordinary and ordinary mode occurs. For special cases of wave incidence, we have coupling to either the extraordinary or ordinary branch. We see these cases in the figure as solid, bold solid, dotted, and dashed curves on the two surfaces. The corresponding incident polarization and wave orientation for each of these special cases is directly indicated. Note that the azimuth ϕ is defined in Fig. 7.

normals for a general uniaxial medium, in Appendix B. In Appendix C, we recap the 4×4 transfer matrix method (developed by Yeh[33]) that we employ to precisely calculate the expected transmission through a uniaxial composite for arbitrary illumination.

We will consider a certain plane of incidence as shown in Fig. 7 with the electric field either parallel [Fig. 7(a)] or perpendicular [Fig. 7(b)] to the plane of incidence, designated as P and S polarization, respectively. We consider a PC of thickness $L = 20a$, and compare the actual transmission versus frequency as calculated from the numerical TMM with the transmission corresponding to a homogenized uniaxial effective medium, calculated with the methodology of Appendix C. We remind the reader that the band structure extracted homogenized medium covered the entire range of effective medium validity for E waves and H waves, respectively. So we will consider an effective uniaxial medium with permittivity tensor of Eq. (3) with $\varepsilon^{E,H} = n_p^2$, where the phase index is extracted from the band structure for E waves and H waves, respectively [see corresponding inset figures in Fig. 2(b) and 3(b)].

In Fig. 9 we show such results for P polarization for four different selected cases of off-plane incident illumination: (i) $\psi = 20^\circ$, $\varphi = 90^\circ$; (ii) $\psi = 70^\circ$, $\varphi = 90^\circ$; (iii) $\psi = 20^\circ$, $\varphi = 60^\circ$; (iv) $\psi = 70^\circ$, $\phi = 60^\circ$. The solid lines represent the actual TMM results, while the solid lines with circles the band structure extracted homogenized medium results. We have done the same calculation for S waves (not shown here). By analyzing all cases, the conclusion is common. The

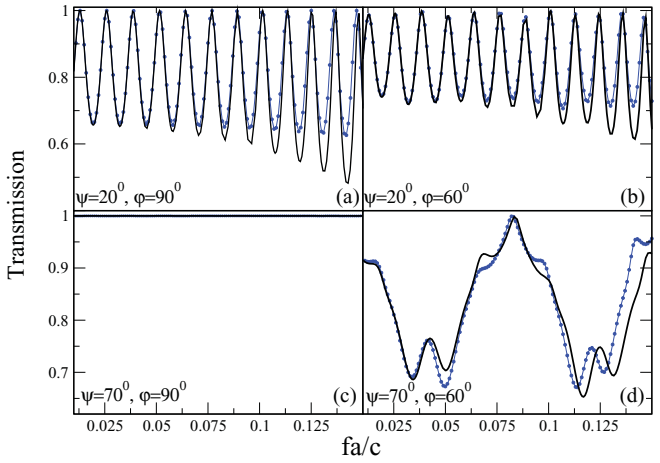

FIG. 9. (Color online) Transmission vs dimensionless frequency fa/c through a 2D PC for out-of-plane incidence and P polarization. Different incident orientations are considered and indicated inside panels (a) through (d). The orientation angles ψ and ϕ are defined in the schematics of Fig. 7. The transmission through the actual PC is calculated with Pendry's TMM method (Ref. 26) and is shown as the solid lines in the figures. For comparison, we calculate the transmission for an equivalent homogenized medium with the method presented in Appendix C. The corresponding result is shown with the solid lines with circles for optical parameters extracted from the E-wave and H-wave PC band structures [seen in inset of Figs. 2(b) and 3(b), respectively].

frequency range of agreement of the actual and homogenized medium result varies with polarization and illumination angle. However, we always see agreement for frequencies up to $fa/c = 0.08$, which was the predicted overlapping range of excellent effective medium validity for E waves and H waves.

To resume, the effective medium picture for an arbitrary orientation is valid for the frequency region where the effective medium picture is valid for both E waves and H waves. In addition, we have observed that traditional EMTs may not always accurately describe effective medium behavior. Accordingly, in the following we characterize effective medium behavior of the 2D polar material composites with the angle test.

III. 2D POLARITONIC PHOTONIC CRYSTALS: EVALUATING THEIR BEHAVIOR AS EFFECTIVE UNIAXIAL METAMATERIALS

We consider two different polaritonic PC structures, both consisting of rods with radii, R equal to $R = 0.30a$, with a being the lattice constant, in a 2D square lattice arrangement. The first PC consists of NaCl (salt) rods in a silicon (Si) matrix, while the second one comprises LiF rods in a NaCl matrix. For the polar materials, i.e., NaCl and LiF, we assume a Lorentzian model for the permittivity function $\varepsilon(\omega)$; i.e.,

$$\varepsilon(\omega) = \varepsilon_\infty \left(1 + \frac{\omega_L^2 - \omega_T^2}{\omega_T^2 - \omega^2 - i\omega\Gamma}\right). \tag{10}$$

The parameters in the Lorentzian permittivity function expressed in Eq. (10) were obtained for both NaCl and LiF by fitting to the actual experimental values, tabulated in Ref. 40. From such fitting we obtained for NaCl $\varepsilon_\infty = 2.22$,

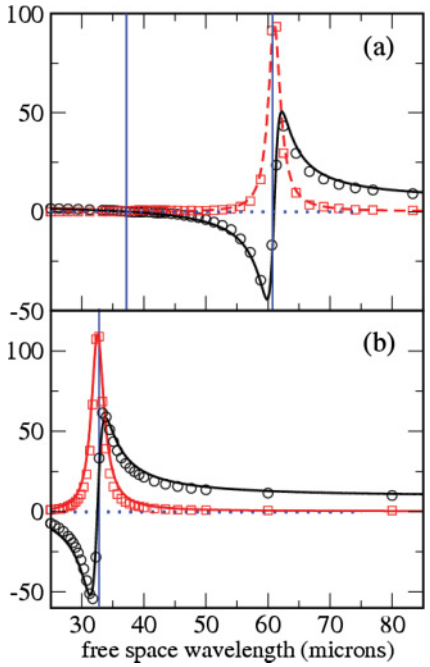

FIG. 10. (Color online) Lorentzian fit for the real part (dark lines) and imaginary part (light-colored lines) of the permittivity ε for NaCl [panel (a)] and LiF [panel (b)]. The circles and squares represent the corresponding experimental values as tabulated in Ref. 40. The vertical lines bound the spectral region with $\varepsilon < 0$ known as the polariton gap (part of region shown for the LiF case).

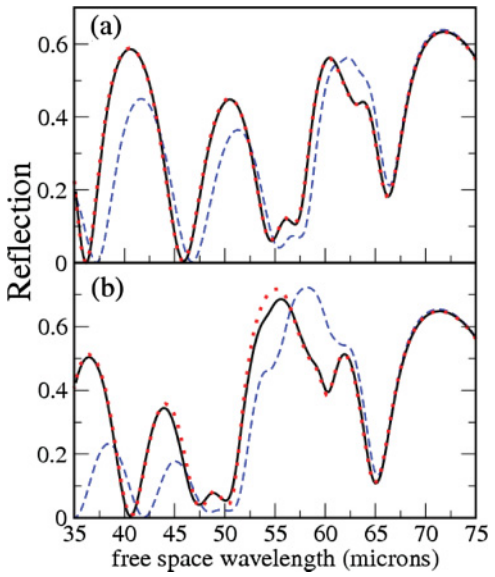

FIG. 11. (Color online) Panel (a) [(b)] shows reflection of E waves (H waves) at normal incidence on the 2D NaCl/Si square polaritonic PC vs free-space wavelength. The dotted line represents theoretical prediction assuming the PC behaves as an effective medium with permittivity obtained from field-averaging (Maxwell-Garnett) theory [see Eq. (1) [Eq. (2)] and Fig. 12]. The bold solid line and dashed lines are the TMM numerical results for the structures with building block size of 1 and 5 μm, respectively.

$\omega_T = 30.90$ THz, $\omega_L = 50.37$ THz, and $\Gamma = 1.20$ THz.[41] Conversely for LiF we have $\varepsilon_\infty = 1.04$, $\omega_T = 57.98$ THz, $\omega_L = 174.22$ THz, and $\Gamma = 4.40$ THz. We plot the real and imaginary parts of the permittivity versus the free-space wavelength, so we are able to easier compare the free-space wavelength of light with the size of the elementary building blocks that we will consider in the following.

The results are shown in Figs. 10(a) and 10(b), respectively. The circles (squares) represent the real (imaginary) parts of the experimentally extracted permittivities as tabulated in Ref. 40. The corresponding dark- and light-colored solid lines represent the Lorentzian fit values from Eq. (10). The vertical lines in Fig. 10 signify the region of prohibited propagation within the bulk polar materials (the permittivity, $\varepsilon < 0$). Such spectral region is also known as the polariton gap (only part of the polariton gap region is shown for the case of LiF). The polariton gap of LiF is close to the NaCl, but lies at higher frequencies. We will focus our investigation on a spectral region roughly encompassing the polariton gap of NaCl, between 35 and 75 μm, which falls in the THz regime. In this regime, Si has an almost flat permittivity equal to $\sim$11.56 and a negligible imaginary part, which we will ignore in our calculations.

We explore in the following whether the proposed polaritonic PCs can behave as an effective isotropic medium for the respective cases of E waves and H waves (see Fig. 1) and the frequency region of interest. If this is true, our analysis in Sec. II suggests that the entire composite structure would behave as a bulk effective uniaxial metamaterial for any arbitrary incident angle. This offers the possibility for unique dispersion engineering of the ordinary and extraordinary propagating waves beyond the capabilities of natural materials. Since our wavelength of interest is targeted around the NaCl polariton gap region, for each types of polar PCs we will consider two different structures. These will have identical composition, the same relative geometric features (i.e., square lattice of rods with radius $R = 0.3a$ with a being the building block size), but a different building block size a. PCs with dispersive constituents cease to have scalable properties, so an analysis in dimensionless units does not apply—the actual size of the building block must be known.[24]

Specifically, we take $a = 1$ μm for the first structure and $a = 5$ μm for the second structure. We consider then EM waves incident normally through 25 building blocks of the first structure and 5 building blocks of the second structure, so that the wave travels through the same polaritonic composite material thickness. We calculate numerically with TMM[26] the reflection through these structures. The TMM reflection results for the NaCl/Si composite are shown in Fig. 11(a) for E waves and in Fig. 11(b) for H waves. The solid lines represent the case for the structure with 1 μm building block size while the dashed lines the structure with 5 μm building block size. We also show for comparison as dotted lines the theoretical reflection value corresponding to a homogenized medium 25 μm thick, as calculated from formula (A2) given in Appendix A. We assume a permittivity predicted from field-averaging EMT [Eq. (1)] for E waves and Maxwell-Garnett theory [Eq. (2)] for H waves. These effective permittivities for the NaCl/Si composite are shown in Fig. 12. The corresponding reflection comparisons and EMT permittivities for the LiF/NaCl composite are seen in Figs. 13 and 14, respectively.

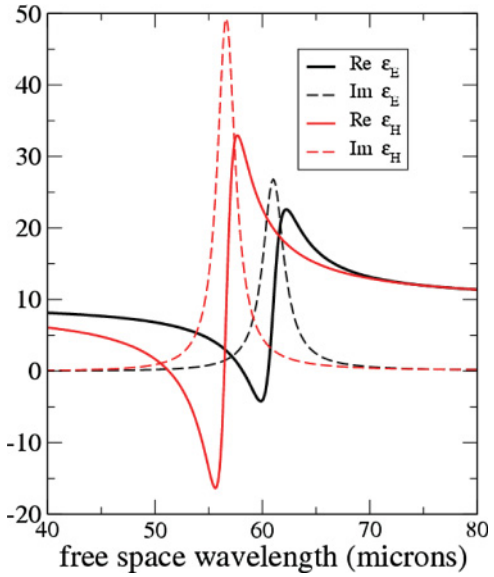

FIG. 12. (Color online) EMT permittivities for the NaCl/Si polaritonic composite vs free-space wavelength. The dark lines correspond to the field-averaging result (ε^E), applicable to E waves, while the light-shaded lines correspond to the Maxwell-Garnett result (ε^H), applicable to H waves. The solid (dotted) lines represent the real (imaginary) parts of the aforementioned quantities.

We see that both NaCl/Si and LiF/NaCl composites with building block size of 1 μm behave excellently as bulk effective media according to field-averaging (Maxwell-Garnett) theory for the case of E waves (H waves). However, for the polaritonic PCs with a building block size of 5 μm, we observe obvious discrepancies between the actual and the effective medium predicted results. This does not necessarily mean that these composites do not behave as effective media. We therefore turn

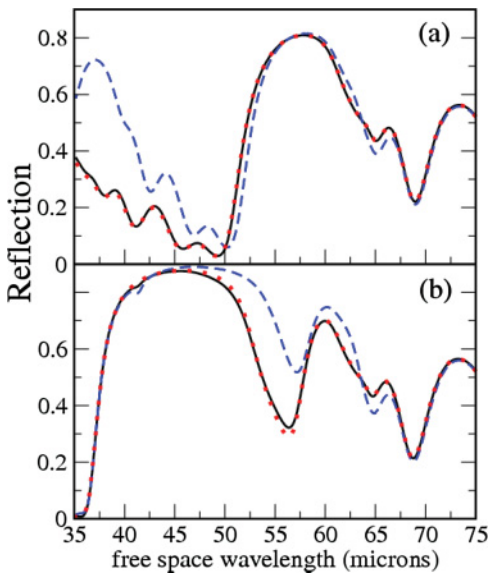

FIG. 13. (Color online) Same as in Fig. 11 but for the LiF/NaCl composite. The theoretical predictions for the permittivities used for the transmission spectra indicated with dotted lines are shown in Fig. 14, for both E waves and H waves.

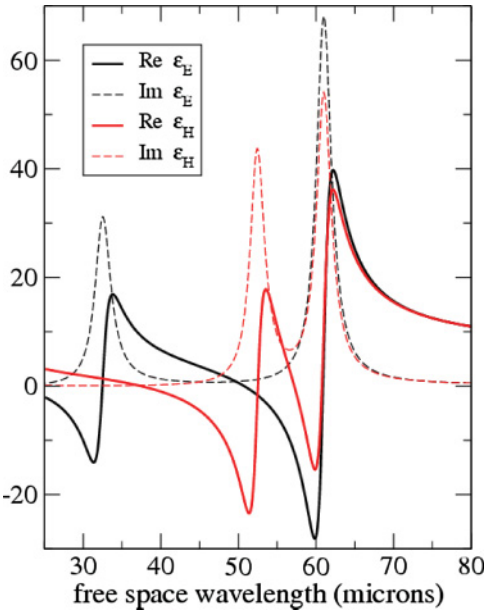

FIG. 14. (Color online) Same as in Fig. 12, but for the LiF/NaCl composite.

to the angle test developed in Sec. II to characterize effective medium behavior.

Equations (8) and (9) representing the angle test are general and should thus be appropriate for fingerprinting effective medium behavior even for composites with lossy constituents. We confirm this by applying such test for the NaCl/Si composite with 1 μm building blocks. The reflection behavior seen in Fig. 11 for this case suggests that we should expect that composite to behave as a bulk effective medium. We calculate $B(\theta_I)$ from Eqs. (8) and (9), with θ_I being the angle of incidence. We do this for two different thicknesses L equal to $5a$ and $7a$, with a representing the building block size of the polaritonic PC, and for the cases of both E waves and H waves. Indicatively, we show in Fig. 15 the case for E waves at 40 μm incident wavelength. We can identify in the figure clearly the characteristic $\sin^2$ effective medium picture signature.

We uncovered such signature for the most part of the targeted frequency regime of interest, for the NaCl/Si composite with 1-μm-sized building blocks. However, for certain frequencies, it was not possible to recover the characteristic $\sin^2$ signature for either or both polarizations. The reason for this is the following. From the wave dispersion relation we have

$$\frac{c^2}{\omega^2}\mathrm{Re}[(k_z^{E,H})^2] = \mathrm{Re}(\varepsilon^{E,H}) - \sin^2\theta_I. \tag{11}$$

However, around frequencies where media become highly lossy, $\mathrm{Re}(\varepsilon^{E,H})$ can become very large and accordingly $\sin^2\theta_I$ would be much much smaller than $\mathrm{Re}(\varepsilon^{E,H})$. In such cases, it would not be possible to uncover the $\sin^2\theta_I$ signature, even when it exists. This is because the $\sin^2\theta_I$ magnitude becomes comparable to the numerical error of the extracted large $\mathrm{Re}(\varepsilon^{E,H})$ value. So, a supplementary angle test criterion

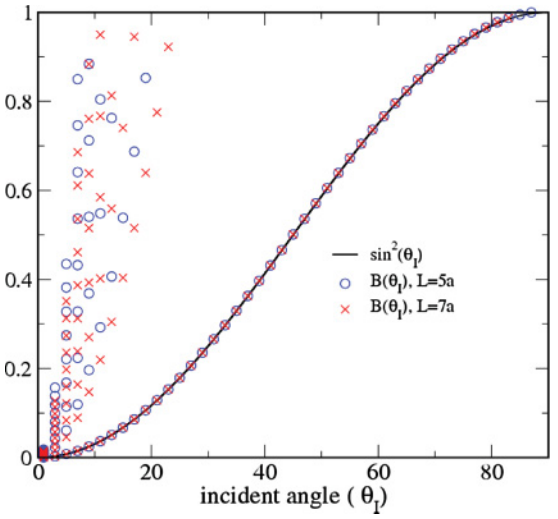

FIG. 15. (Color online) Angle test for E-wave propagation at free-space wavelength of 40 μm for the NaCl/Si PC with building block with size $a = 1$ μm. The branches l, of the angle test function $B(\theta_I)$ defined in Eq. (8), are calculated vs incident angle θ_I for two PC thicknesses L. The results for $L = 5a$ are shown with the circles while the results for $L = 7a$ are shown with the x's. We find the existence of a common branch for the $L = 5a$ and $L = 7a$ cases which in addition follows a $\sin^2$ function in terms of θ_I (solid line). The latter is the fingerprint of effective medium behavior.

is required in order to treat these cases. From the same wave dispersion relation we have that

$$\frac{c^2}{\omega^2}\mathrm{Im}\left[(k_z^{E,H})^2\right] = \mathrm{Im}(\varepsilon^{E,H}). \tag{12}$$

So, Eq. (12) becomes for both polarizations

$$\frac{c^2}{\omega^2 L^2}\,\mathrm{Im}\left[\left(\cos^{-1}\frac{\left(\frac{r}{t}\right)_{2L}}{2\left(\frac{r}{t}\right)_L} + \; l\pi\right)^2_{\theta_I}\right] = C(\theta_I) = C, \tag{13}$$

with $\cos^{-1}$ designating the principal value l, the branch order, and $C(\theta_I)$ designating the constant function. Equation (13) can serve as a supplementary angle test criterion, for cases where failure to obtain the $\sin^2$ signature is due to large permittivity values. It follows from Eq. (13) that for a homogeneous medium, the function $E(\theta_I)$ given below,

$$E(\theta_I) = \frac{2\pi c^2}{\omega^2 L^2}\left\{\mathrm{Im}[\Delta(\theta_I)]\mathrm{Re}[\Delta(\theta_I)]/\pi + l\,\mathrm{Im}[\Delta(\theta_I)]\right\}, \tag{14}$$

where

$$\Delta(\theta_I) = \left(\cos^{-1}\frac{\left(\frac{r}{t}\right)_{2L}}{2\left(\frac{r}{t}\right)_L}\right)_{\theta_I}, \tag{15}$$

is a constant function versus the incident angle θ_I. We will investigate accordingly the constant profile of the $E(\theta_I)$ function and shall call this test the "flat-profile angle test" in the following.

An example is the case chosen in Fig. 16, corresponding to E waves through the NaCl/Si composite for a free-space

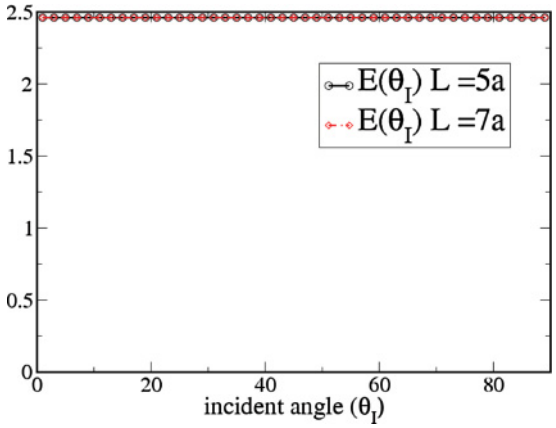

FIG. 16. (Color online) Flat-profile angle test for E-wave propagation at free-space wavelength of 65 μm for the NaCl/Si PC with building block with size $a = 1$ μm. The large, effective permittivity value does not allow us to recover the $\sin^2$ signature. We see however the clear constant function $E(\theta_I)$ vs incident angle for two different lengths of $L = 5a$ and $L = 7a$, confirming effective medium behavior.

wavelength of $\lambda = 65$ nm. We were not able to recover the $\sin^2$ signature, but the structure clearly satisfies the flat-profile angle test criterion, as we can clearly see in the figure. One must seek the common branch of $E(\theta_I)$ for the two thicknesses of $L = 5a$ and $L = 7a$. In general, this can emanate from a different branch order l in Eq. (13). In Fig. 16, we show such common branch which in this particular case corresponds to $l = 0$, for both thicknesses. Equation (12) implies that the constant value of the $E(\theta_I)$ function for the common branch solution should yield the imaginary part of the effective permittivity. Indeed, Fig. (16) suggests an $\mathrm{Im}(\varepsilon^E)$ value of 2.46, which is in excellent agreement with the value of 2.43 predicted from EMT.

We found that the flat-profile angle test criterion proved particularly useful for the LiF/NaCl composite. Both constituents of this composite are highly lossy resonant material, so one would expect to have high permittivity values pretty much throughout the frequency range of interest. In particular, when investigating the LiF/NaCl composite with 1-μm-sized building blocks, mostly we found it was not possible to characterize it with the $\sin^2$ angle test. However, as expected by the agreement of the reflection spectra with EMT, the structure demonstrates a constant profile in $E(\theta_I)$, thus satisfying the criterion of the flat-profile angle test of Eq. (14).

We turn our attention now to the characterization of the composites with 5-μm-sized building blocks, where in the reflection spectra of Figs. 11 and 13 we have identified apparent departures from the results predicted from the field-averaging and Maxwell-Garnett theory, respectively. We do this to understand whether such discrepancies signify effective medium breakdown, or the limitation of such aforementioned theories. We first characterize the NaCl/Si composite. We do so by employing in synergy both the $\sin^2$ and the flat-profile angle test. We will start by applying first the $\sin^2$ criterion. If the structure fails to demonstrate the $\sin^2$ signature then we proceed in applying the flat-profile angle test. If a flat-profile signature is recovered, this would ascertain effective medium

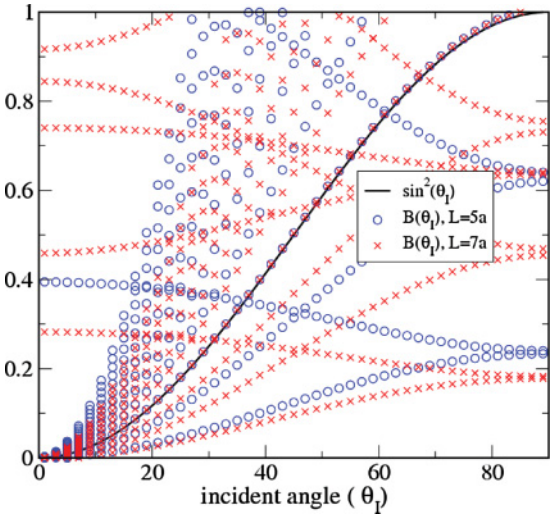

FIG. 17. (Color online) Same as Fig. 15 but for E-wave propagation at free-space wavelength of 50 μm for the NaCl/Si PC with building block with size $a = 5$ μm.

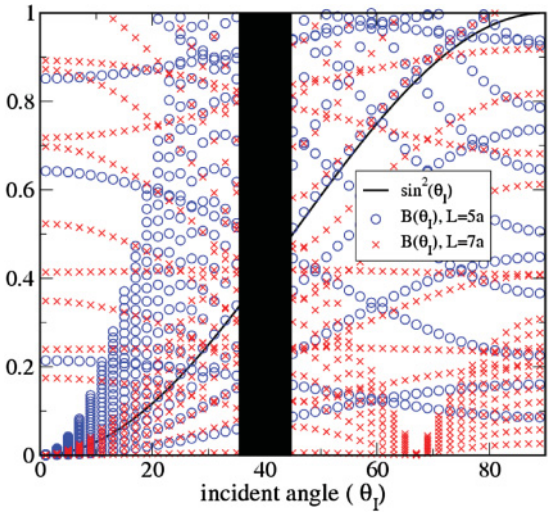

FIG. 18. (Color online) Angle test for E-wave propagation at free-space wavelength of 40 μm for the NaCl/Si PC with building block with size $a = 5$ μm. The circles, x's, and solid lines represent the same quantities as in Figs. 15 and 17. The blocked region is a region with very small r/t values (Ref. 27). We find the existence of two respective branches for the $L = 5a$ and $L = 7a$ cases. We start seeing an apparent difference between the values of the aforementioned branches and an obvious small deviation from the $\sin^2\theta_I$ function. This alerts us that the quality of the effective medium picture has degraded at these frequencies.

validity. Otherwise, we will conclude that an effective medium description would not be appropriate for the case under consideration.

For E waves with free-space wavelength of 50 μm we find two common branch solutions l of the function $B(\theta_I)$, which agree well with each other and are close to the $\sin^2(\theta_I)$ function. We show this in Fig. 17. In other words, the angle test ascertains that the effective medium picture works reasonably well at such frequency. Now, if we move to shorter wavelengths of 40 μm we observe two branch solutions that are close to each other, but the difference between them and with the $\sin^2$ function becomes apparent (see Fig. 18). So a wavelength of 40 nm signifies a a rough limit where the validity of the effective medium picture degrades for E waves propagating through the NaCl/Si PC with 5-μm-sized building blocks. Conversely, for the case of H waves we could not recover the $\sin^2$ signature in the frequency range of interest. For the most part of the spectrum, we could not obtain a flat-profile signature either, which alerts us to an effective medium picture breakdown.

Now we repeat the same tests for the LiF/NaCl polaritonic PC with 5-μm-sized building blocks for E waves and H waves. The structure does not give a $\sin^2$ signature for most parts of the spectrum of interest, but we uncovered a flat-profile signature in all cases. This means that the LiF/NaCl polaritonic PC with 5 μm still behaves as an effective medium despite the discrepancies in the reflection spectra with the theoretical expectations from a permittivity response according to field-averaging and Maxwell-Garnett theory. The case of E-wave propagation through the NaCl/Si composite at about 60 μm free-space wavelength also demonstrated such discrepancy, while the criteria we established did ascertain that the structure should behave as an effective medium in this wavelength.

One major advantage of establishing these angle test criteria is to be able to determine whether EM parameter retrieval processes[42–44] yielding the medium's constitutive parameters are meaningful. In order to demonstrate this and to understand the observed deviations from the traditional EMTs in certain cases, we will perform such retrieval process in the NaCl/Si and LiF/NaCl PC composites. The standard EM retrieval process involves the evaluation of the permittivity and permeability of a metamaterial, with the use of the reflectivity r and transmissivity t.[42,43] Here we will follow an alternative methodology for the retrieval of the constitutive parameters, which is based on employing the ratio of reflectivity over transmissivity r/t, which we obtain in the numerical transfer matrix method.[26] We keep the process general allowing for the possibility of existence of magnetic behavior, i.e. permeability different from 1. The detailed steps of the methodology we apply are given in Appendix D.

In all cases where the structure demonstrates an effective medium signature, we were able to recover constitutive parameters that are independent of the thickness of the structure. It is not surprising to find that in the cases where we were not able to find an effective medium signature with the established tests (either $\sin^2$ angle test or flat-profile angle test), it was not possible to retrieve length-independent constitutive parameters. The retrieval was performed by employing the numerical r/t TMM values for thicknesses $L = 5a, 7a$, and $10a$, where a represents the size of the building block.

Both types of 1-μm-sized building block structures (NaCl/Si and LiF/NaCl) yielded magnetic permeability equal to $\sim$1, and effective permittivity in most excellent agreement with the predictions of field-averaging theory for the case of E waves, and Maxwell-Garnett theory for the case of H waves. The NaCl/Si with 5-μm-sized building blocks behaves as an effective medium only up to 50 μm free-space wavelength and E waves. For the latter cases, we performed the retrieval

process and found also an effective magnetic behavior. We show the retrieved constitutive EM parameters in Fig. 19, with permittivity depicted in panel (a) and permeability in panel (b). Solid lines with circles represent the real part of the latter quantities, while solid lines with diamonds represent the respective imaginary parts. Again we show for comparison the field-averaging prediction for the permittivity, with dashed (dotted) lines for the real (imaginary part). In panel (c) we depict also the retrieved refractive index n represented with solid lines with circles for the real part and solid lines with diamonds for the imaginary part. We observe that it is different from the effective medium prediction (dashed and dotted lines, respectively) but in excellent agreement with the band structure[45,46] extracted index (light and dark empty squares). Note that the effective medium parameters at the frequency edge of effective medium validity for this structure yield an effective wavelength within the material that is about 3.5 times larger than the structural building block.

We note in Fig. 19 that the frequency region around 60 μm where magnetic behavior appears is where we also find a larger discrepancy between retrieved permittivity and field-averaging EMT permittivity. Remarkably, it was around the same frequency region where the TMM reflection spectra did not match the calculated result from field-averaging EMT predictions. We proceeded in also retrieving the constitutive parameters for the LiF/NaCl PC with 5-μm-sized building blocks. Our observations are very similar to the case of E waves through the NaCl/Si PC with 5-μm-sized building blocks. In particular, we consistently find that the departure from the

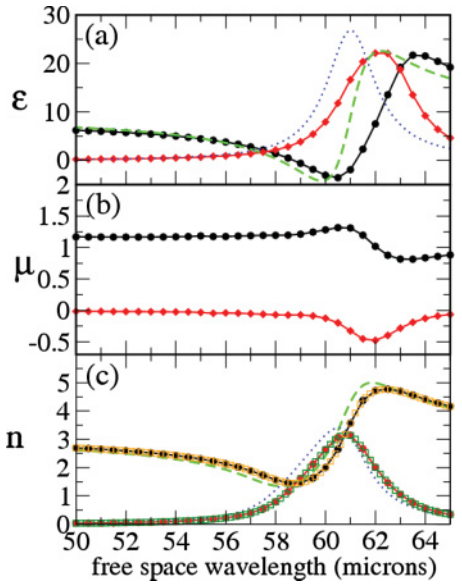

FIG. 19. (Color online) Retrieved permittivity function [panel (a)], permeability function [panel (b)], and refractive index [panel (c)] for E waves through the NaCl/Si composite with 5-μm-sized building block vs the free-space wavelength. The real (imaginary) part of the retrieved parameters is shown as solid lines with circles (solid line with diamonds). For comparison we show the predicted permittivity response function from field-averaging theory. Real (imaginary) part of the latter is shown with dashed (dotted) line. In panel (c) the band structure extracted refractive index is also shown with light (dark) empty squares for the real (imaginary) part.

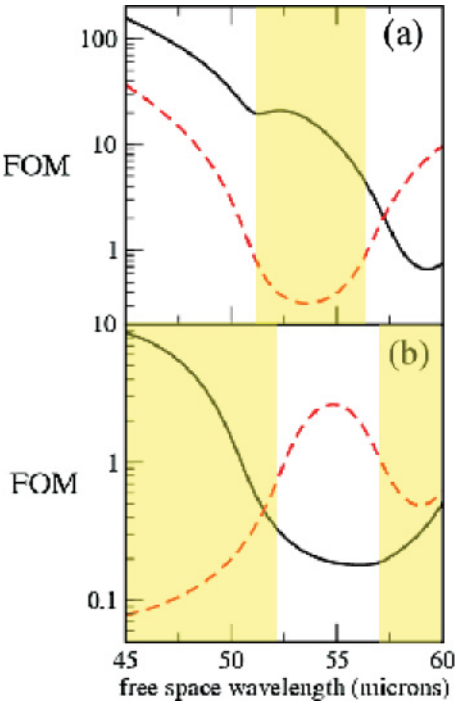

FIG. 20. (Color online) Figure of merit averaged over all illumination angles ψ and ϕ (defined in Fig. 7) vs free-space wavelength. In (a) the result for the NaCl/Si composite is shown. In (b) the result for the LiF/NaCl composite is shown. The solid (dotted) lines represent the figure of merit for the extraordinary (ordinary) wave. The shaded region represents the frequency region with effective $\varepsilon^H < 0$, in each composite.

standard EMTs is accompanied by a small-strength magnetic behavior. Magnetic behavior has been reported to occur before in polaritonic PCs[22,47] and is attributed to the large permittivity contrast between the constituents.[48,49] Incidentally, negative imaginary parts in the permeability function that we observe here are physical and have been reported before.[50]

To recap, the combination of the $\sin^2$ and flat-profile angle-test label efficiently effective metamaterial behavior in 2D composites, even in the presence of high losses. Thus, we have obtained a most valuable criterion determining whether the constitutive parameters obtained from retrieval processes are meaningful. Manmade composites which behave as bulk homogeneous media are particularly attractive metamedia. Owing to their length and angle-independent optical properties, they are expected to give a consistent response, which is of particular importance if they are to be used as components in optical setups. We stress that for the particular case of 2D composites, the angle-test must be satisfied for both E waves and H waves. Only under this condition, the composite would behave as an effective bulk uniaxial metamaterial under arbitrary illumination.

In the following, we focus on 2D polaritonic composites that behave as effective media throughout the frequency region of interest. We have chosen therefore the NaCl/Si and LiF/NaCl composite with a meta-atom size of 1 μm.

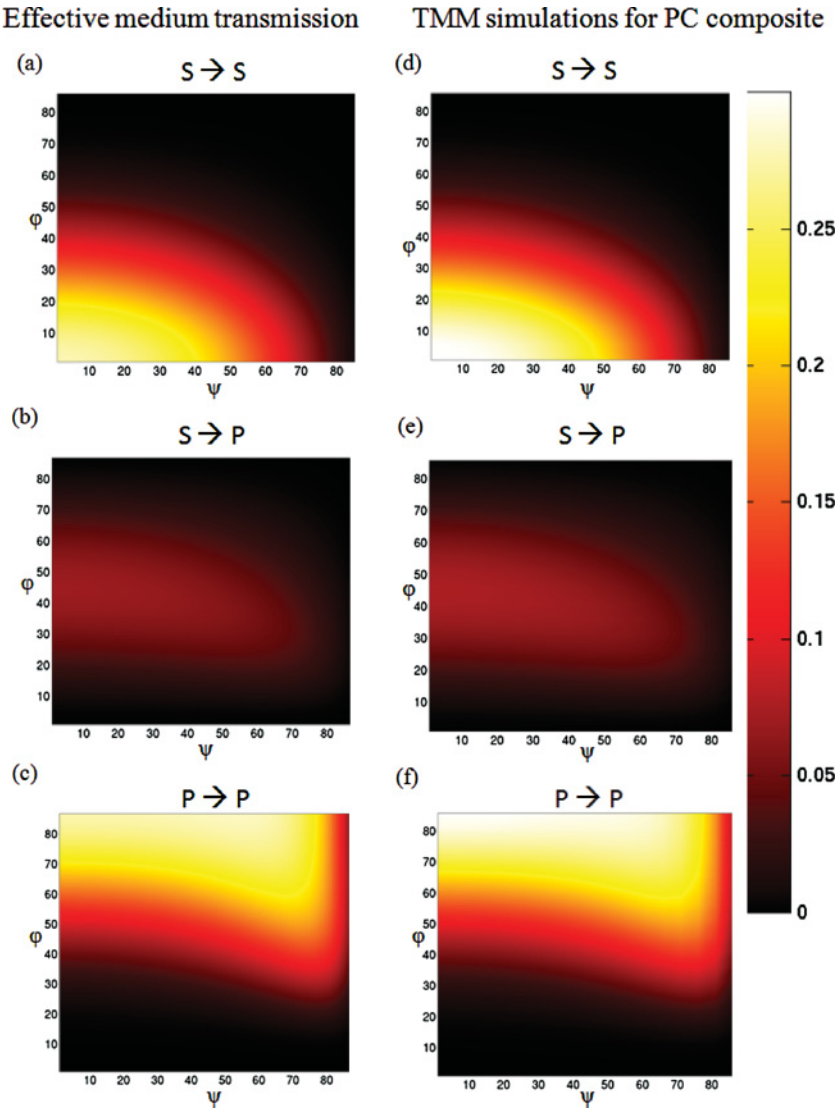

FIG. 21. (Color online) Transmission of an incident wave with wavelength of 55 μm through a 25-μm-thick NaCl/Si polaritonic composite. The transmission is shown vs the angles of incidence ψ and ϕ that are defined in Fig. 7. Transmission is calculated for the homogenized effective medium (results shown in the left column) and for the actual composite with the TMM method (results shown in the right column). Panels (a), (d) represent the transmission for the S polarization to S polarization channel. Likewise panels (b), (e) represents transmission for the S polarization to P polarization channel, and panels (c), (f) represent transmission for the P polarization to P polarization channel.

IV. EXTRAORDINARY TRANSMISSIVE PROPERTIES OF UNIAXIAL 2D POLARITONIC COMPOSITE METAMATERIALS

In the NaCl/Si composite we have prohibited propagation only through one of the constituents (NaCl), while for the LiF/NaCl composite there exists a frequency region where transmission is very low in both bulk LiF and NaCl. It would be very interesting to see the angular behavior of transmission in these composites which is of utmost importance in the construction of optical components such as polarization filters and converters, as well as beam diverters, splitters, lenses, etc. The chosen composites with 1 μm meta-atom size satisfy excellently the standard EMTs. We will calculate therefore the transmission for chosen frequencies and an arbitrary illumination of angle ψ and azimuth ϕ (defined in Fig. 7). We employ for such calculation the 4×4 transfer matrix method which applies to homogeneous anisotropic media (see Appendix C).

For optical parameters we will use the field-averaging permittivity for ε^E and the Maxwell-Garnett permittivity for ε^H. Such effective ε^E and ε^H parameters define the complete permittivity tensor [given by Eq. (3)] and are depicted in Figs. 12 and 14 for the NaCl/Si and LiF/NaCl composites, respectively. We let the angles ψ and ϕ vary between 0° and 90°. We calculate the transmission for a slab thickness of 25 μm along the propagation direction, z (see Fig. 7). This means that the structures are about half a wavelength thick for the frequency region of interest. In each case, we will also calculate the actual transmission for the composite via the numerical transfer matrix method[26] for comparison. With both these methods, we will calculate the part of transmission corresponding to the outgoing wave with the same polarization as the incident wave and the part of transmission corresponding to the outgoing wave with different polarization as the incident wave. Cross-polarization does not occur under the illumination condition of Fig. 1, but can in general occur for an incident wave impinging at an arbitrary direction as seen in Fig. 7. The cross-polarization transmission channel emanates from the simultaneous coupling to both ordinary and extraordinary waves inside the uniaxial material (see Appendix C).

In both the structures, we found negligible transmission for frequencies where both ε^E and ε^H are negative, or in cases where either of the imaginary parts of ε^E and ε^H is high.

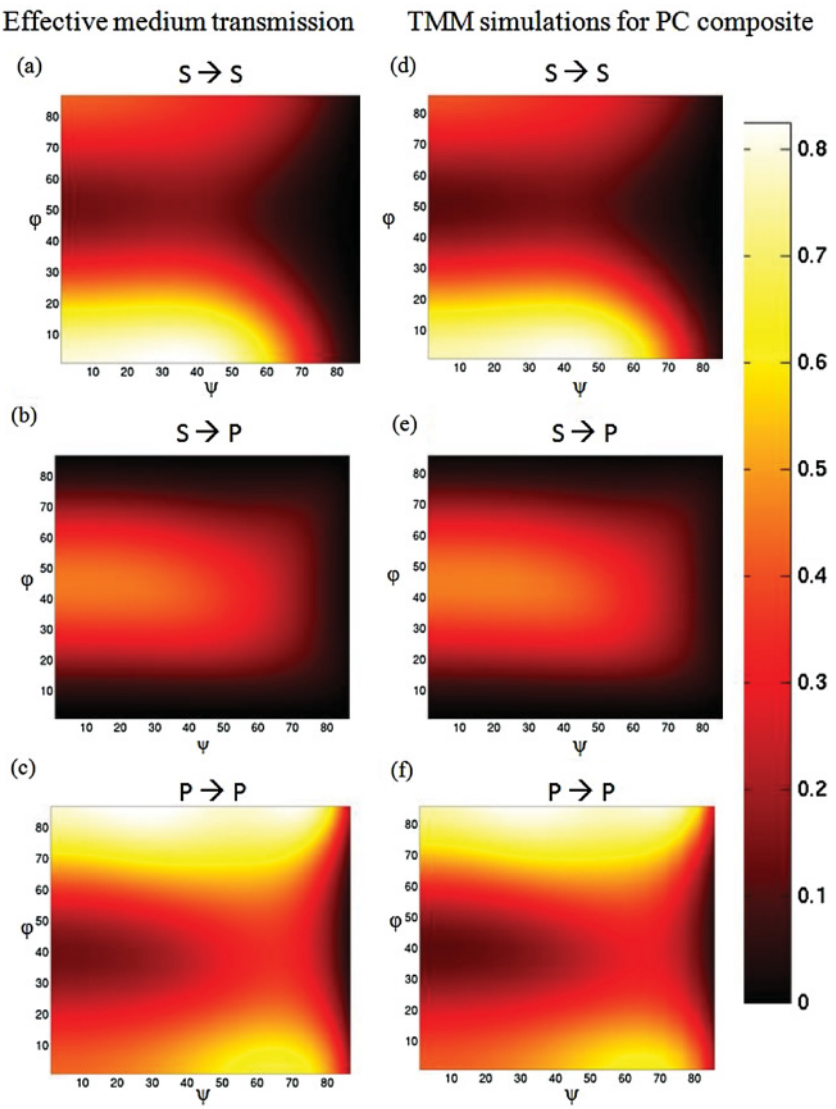

FIG. 22. (Color online) Same as Fig. 21 but for an incident wave with free-space wavelength equal to 45 μm.

Therefore suitable operational frequencies would be those at which at least one of ε^E and ε^H is positive and at the same time both the respective imaginary parts are small. In particular, the pertinent parameter for a good transmissive behavior is the figure of merit (FOM),[51–53] which is given by the ratio $|\mathrm{Re}(k_{2z})|/\mathrm{Im}(k_{2z})$.[54] We can obtain the FOM for the ordinary and extraordinary wave from Eqs. (B1) and (B2), respectively. We show the FOM versus the free-space wavelength in Figs. 20(a) and Figs. 20(b) for the NaCl/Si and LiF/NaCl composites, respectively. The result for the ordinary mode is shown with dotted lines, while the result for the extraordinary mode is shown with solid lines. As we desire unusual transmissive properties, we select to study further certain characteristic cases, where the extraordinary wave is characterized by a large FOM.

For the NaCl/Si composite we have $\varepsilon^E\varepsilon^H < 0$, and a high figure of merit around 55 μm, for only the extraordinary wave. We show the transmission as a function of the illumination angles ψ and ϕ in Fig. 21. In panel (a) we show the transmission channel from an S to S polarized wave. Conversely, in panels (b) and (c) we show the S to P and P to P polarization channels. We do not need to also show the P to S polarization channel as it is the same as the S to P channel because of reciprocity. The corresponding transmissions for the actual composite calculated with the numerical TMM[26] are shown in panels (d), (e), and (f). We observe a remarkably excellent agreement between the two results for the actual and homogenized medium. We see in Fig. 21 a significant transmission around 35% for both S to S and P to P channels, and no possibility for polarization conversion. What is interesting is that if for certain incident angles ϕ, ψ the P to P channel has high transmission, then the S to S channel has negligible transmission and vice versa. This means that this structure can function as a polarization filter yielding S or P polarized waves from an unpolarized source just by changing the direction of incidence onto the structure.

If we move now to a little higher frequency we encounter a region around 45 μm where both ε^E and ε^H are positive with small imaginary parts, although NaCl has a negative permittivity at such frequency. In this case both ordinary

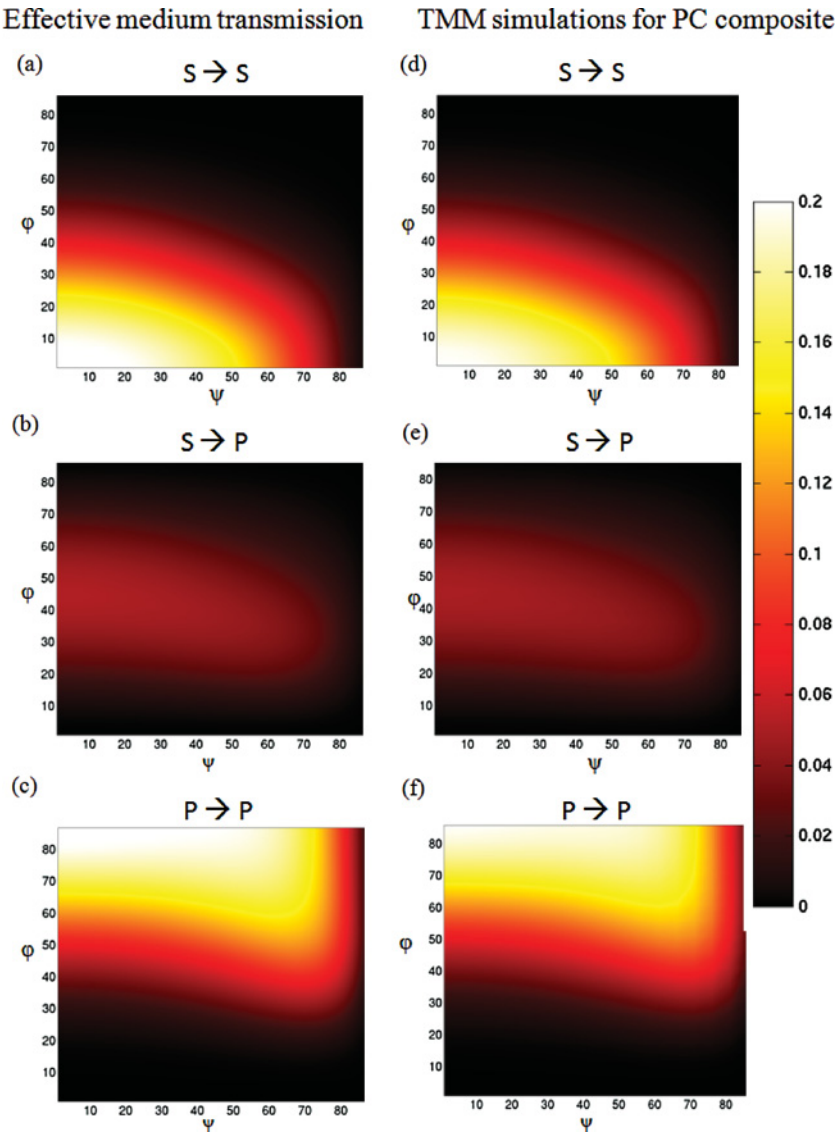

FIG. 23. (Color online) Same as Fig. 21 but for an incident wave with free-space wavelength equal to 45 μm through a 25-μm-thick LiF/NaCl composite structure.

and extraordinary waves have high FOM. We show the transmission as a function of the incident angles in Fig. 22 for all the different transmission channels, which are designated on the top of each respective panel. Also in this case, we show the transmission results for the homogenized medium in the left column and the transmission results for the actual composite structure in the right column. Here too we observe a remarkably excellent agreement between the two results. We find in Fig. 22 transmission values as high as 80% for the S to S and S to P polarization channels. Also, if we choose incidence with ψ close to zero and azimuth ϕ around 45°, the only significant transmission channel with 40% transmissivity is that of S to P or P to S polarization. In other words, the structure acts as a very efficient polarization converter at such frequency.

Finally, it is worth looking at the transmission behavior through the LiF/NaCl composite at 45 μm, where the extraordinary wave has a high FOM. We depict the transmission for the homogenized medium and actual composite for all polarization channels in Fig. 23. We observe in Fig. 23 that the qualitative behavior of the LiF/NaCl metamaterial at 45 μm is the same as the NaCl/Si metamaterial at 55 μm. We emphasize that in such a case it is particularly impressive to find a transmission as high as 20% through the composite structure, when the transmission is next to zero for any angle of incidence through a bulk 25-μm-thick NaCl or LiF slab at such frequency.

The results in this section manifest that mixing polar material with other polar materials or dielectrics is a route of constructing uniaxial metamaterials with completely different transmission behavior from their constituents. The observed anisotropy in the permittivity tensor can be extraordinarily high and includes cases where the elements of the permittivity tensor are of opposite sign (hyperbolic dispersion[11]). Thus these type of composites can be a promising recipe for the construction of optical components operable at the THz spectrum. As we see a distinctively different angular transmission profile between the cases of Figs. 21 and 23 and the case of Fig. 22, it would be particularly interesting to understand more this exotic transmissive behavior of the polaritonic uniaxial metamaterial composites.

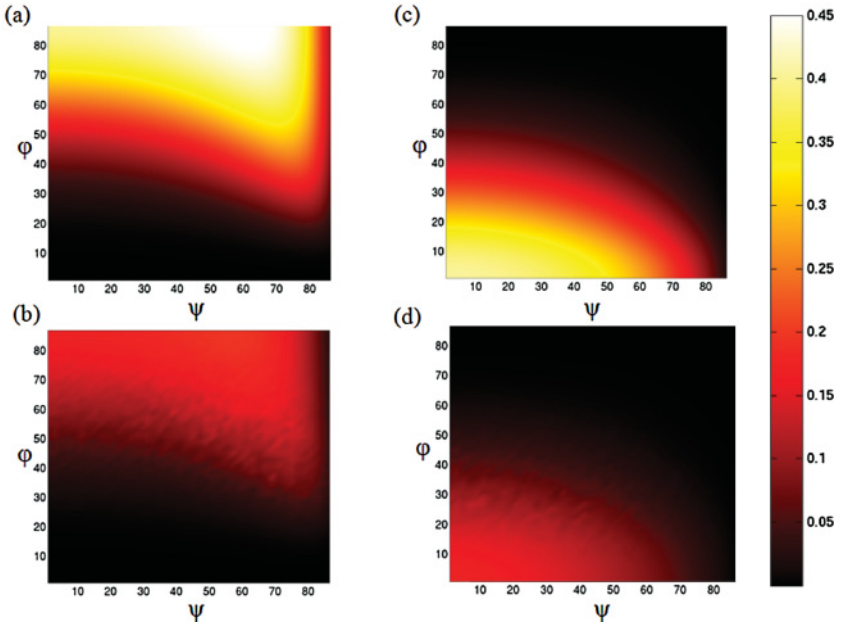

FIG. 24. (Color online) Transmission vs angles of incidence ϕ and ψ (defined in Fig. 7) through the NaCl/Si composite for an incident wave of 55 μm free-space wavelength (homogenized medium result). In (a) and (b) we show the P polarization to P polarization transmission for a 15-μm- and 32-μm-thick composite, respectively. Conversely, in (c) and (d) we show the S polarization to S polarization transmission for a 15-μm- and 32-μm-thick composite, respectively.

V. UNDERSTANDING THE EXOTIC TRANSMISSIVE PROFILE OF THE POLARITONIC UNIAXIAL METAMATERIAL 2D COMPOSITES

We observe a very interesting transmission profile through the polar composite metamaterial structures, which can be exploited for optical component applications as we discussed in Sec. IV. It is therefore particularly interesting to understand the physical origin of the angular transmission map. Strikingly, the angular transmission maps of the NaCl/Si composite at 55 μm wavelength are similar to the transmission maps of the LiF/NaCl composite at 45 μm wavelength. Both are distinctively different from the angular transmission maps of the NaCl/Si composite at 45 μm wavelength.

To understand this further we calculate the angular transmission maps for different thicknesses for the NaCl/Si composite at 55 μm wavelength. We show such angular transmission map in Fig. 24. In panels (a) and (b) we show the result for the P to P polarization channel for thicknesses of 15 and 32 μm, respectively. Conversely, in panels (c) and (d) we show the result for the S to S polarization channel for thicknesses of 15 and 32 μm. We compare these with the respective results in Figs. 21(c) and 21(a) for a 25-μm-thick NaCl/Si composite. We observe that while the actual magnitude of transmission changes, the morphology of the angular transmission maps is insensitive to the thickness of the structure. The same holds true for the S to P polarization channel as well (not shown here). We calculated the angular transmission maps for various thicknesses also for the LiF/NaCl composite at 45 μm wavelength. We also observed in such a case a thickness-insensitive morphology of the angular transmission maps for all polarization channels.

Now, we move to the NaCl/Si composite at 45 μm wavelength. Here we find a completely different behavior. We find angular transmission maps with morphology changing drastically with the thickness of the structure for all polarization channels. Indicatively, we show the angular transmission map for the P to P polarization channel in Fig. 25. Panel (a) corresponds to a thickness of 15 μm and panel (b) corresponds to a thickness of 32 μm. Note also the result for a thickness of 25 μm that was depicted in Fig. 22(c). We observe there a dramatic change in the morphology of the angular transmission maps, when we increase the thickness from 15 μm to 25 μm. We observe a smaller change in the morphology when the structural thickness in increased from 25 μm to 32 μm. The same observations hold for the S to S polarization channel, while the S to P polarization channel seems to show a smaller sensitivity on the structural thickness.

The reason that we find the same qualitative behavior of the transmission maps for the case of the NaCl/Si composite at 55 μm wavelength and the case of the LiF/NaCl composite at 45 μm wavelength, but different from the case of the NaCl/Si composite at 45 μm wavelength is the following. The former cases have $\mathrm{Re}(\varepsilon^E) > 0$, $\mathrm{Re}(\varepsilon^H) < 0$, and a high FOM only for the extraordinary mode. This means that for these cases, the ordinary wave survives through the structure only for a finite skin depth of the order of $1/\mathrm{Im}(k_O)$, with k_O being the ordinary wave vector along z, given by Eq. (B1). So essentially, we have single-beam propagation after $\sim$2 μm, $\sim$3.5 μm for the NaCl/Si composite at 55 μm and for the NaCl/LiF composite at 45 μm, respectively. On the other hand, $\mathrm{Re}(\varepsilon^E) > 0$ and $\mathrm{Re}(\varepsilon^H) > 0$ for the NaCl/Si composite at 45 μm wavelength. So in such case transmission is birefringent, with both ordinary and extraordinary modes coexisting. The thickness dependence of the angular morphology in the latter case emanates from the thickness dependence of the relative acquired phase between these two modes as they propagate through the structure.

In the following, we will try to understand the particular morphology of the angular transmission maps that is common for the case of the NaCl/Si composite at 55 μm wavelength and the LiF/NaCl composite at 45 μm wavelength. Is the observed similarity in the morphology of the transmission maps coincidental, or should we expect to find it in any uniaxial metamaterial with $\mathrm{Re}(\varepsilon^E) > 0$ and $\mathrm{Re}(\varepsilon^H) < 0$?

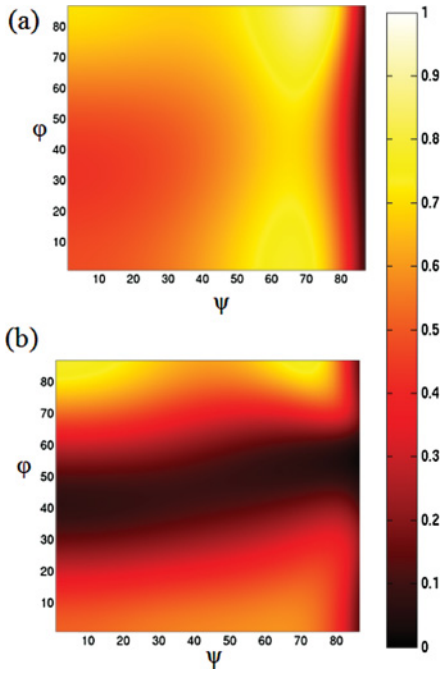

FIG. 25. (Color online) Transmission vs angles of incidence ϕ and ψ (defined in Fig. 7) through the NaCl/Si composite for the P polarization to P polarization channel for an incident wave of 45 μm free-space wavelength (homogenized medium result). In (a) we show the transmission through a 15-μm-thick composite while in (b) the transmission though a 32-μm-thick composite.

The coupling efficiency of the incident wave with the extraordinary mode is proportional to the alignment between their respective polarization. This implies that

$$c_{\text{eff}}^{SS} \propto |\hat{p}_S \cdot \hat{p}_{EO}|^2 \tag{16}$$

and

$$c_{\text{eff}}^{PP} \propto |\hat{p}_P \cdot \hat{p}_{EO}|^2, \tag{17}$$

with c_{eff}^{SS} and c_{eff}^{PP} representing the coupling efficiencies for the S to S and P to P polarization channels, respectively. It is easy to show with the use of Eqs. (C7)–(C14), together with Eqs. (B3)–(B4), that c_{eff}^{SS} has a $\cos^2\phi$ angular envelope, while c_{eff}^{PP} has a $\sin^2\phi$ angular envelope. This is consistent with our observation in the angular transmission maps, where we find the S to S polarization channel to be dominant for small azimuth angles ϕ, and the P to P polarization channel to be dominant for large azimuth angles ϕ.

In addition, we observe a highly insensitive profile with the angle ψ for the following reason. The cases of Figs. 21 and 23 have $|\varepsilon^H|$, $|\varepsilon^E|$ quite larger in comparison to 1. In these cases, the wave vector k_{2z} of the extraordinary mode—obtained from Eq. (B2)—is dominated by the nonangular terms. For other frequencies, with also $\text{Re}(\varepsilon^E) > 0$ and $\text{Re}(\varepsilon^H) < 0$, where $|\varepsilon^H|$, $|\varepsilon^E|$ are comparable or smaller than 1, we find a strong angular dependence on k_{2z}. In particular, we have large $\text{Im}(k_z)$ values where both ϕ and ψ are large in such cases. This does not influence much the angular map of the transmission for the S to S polarization channel. However, for the P to P polarization channel we find high transmission to be concentrated toward small ψ angles.

VI. CONCLUSIONS

We have studied metamaterial behavior for 2D composites composed of dielectric-polar or polar-polar material constituents. The objective is to obtain composite metamaterials that are highly suitable for the construction of THz optical components. For this purpose, we have constructed a reliable test that characterizes whether the composite behaves like a bulk homogeneous uniaxial medium. We believe that such test will aid the development of related criteria in 3D bulk metamaterials which are in general bianisotropic.[55] Based on the developed test, we have analyzed different 2D composites and selected certain structures behaving as a uniaxial homogeneous medium.

We found that polar-media-based uniaxial metamaterials with both $\text{Re}(\varepsilon^H)$ and $\text{Re}(\varepsilon^E)$ positive have high FOM for both ordinary and extraordinary modes. The angular transmission map is thickness dependent, so the particular thickness must be taken into account in optical device design. We have found a particular case where the uniaxial metamaterial composite functions as a polarization converter. On the other hand, uniaxial metamaterials with $\text{Re}(\varepsilon^E)$ positive and $\text{Re}(\varepsilon^H)$ negative, and respective magnitudes large in comparison with 1, have a characteristic angular transmission map that is independent of the thickness of the metamaterial. In particular, such cases have transmission that is high for many angles, with either only the S to S or the P to P polarization channel contributing. Therefore, these structures can operate as efficient THz polarization filters.

ACKNOWLEDGMENTS

This work was partially supported by EU projects ENSEMBLE, ECONAM, and PHOME and Ames Laboratory (Contract No. DE-AC0207CH11385).

APPENDIX A: TRANSMISSION AND REFLECTION THROUGH A HOMOGENEOUS UNIAXIAL SLAB: PLANE OF INCIDENCE NORMAL TO THE OPTICAL AXIS

We consider the illumination conditions of Fig. 1, with respect to the optical axis y (which corresponds to the rod axis of the 2D homogenized composite). We have that the transmission coefficient will be given by[36]

$$T^{E,H} = \frac{1}{\frac{1}{4}\left|2\cos k_{2z}^{E,H} L - i\left(\chi^{E,H} + \frac{1}{\chi^{E,H}}\right)\sin k_{2z}^{E,H} L\right|^2}, \tag{A1}$$

the reflection coefficient by

$$R^{E,H} = \frac{\frac{1}{4}\left|\left(\chi^{E,H} - \frac{1}{\chi^{E,H}}\right)\sin k_{2z}^{E,H} L\right|^2}{\frac{1}{4}\left|2\cos k_{2z}^{E,H} - i\left(\chi^{E,H} + \frac{1}{\chi^{E,H}}\right)\sin k_{2z}^{E,H} L\right|^2}, \tag{A2}$$

and the complex reflectivity/transmissivity ratio by

$$\left(\frac{r}{t}\right)_L^{E,H} = \frac{i}{2}\left(\chi^{E,H} - \frac{1}{\chi^{E,H}}\right)\sin k_{2z}^{E,H} L. \tag{A3}$$

The superscripts E and H refer to the cases of E waves and H waves, respectively. $k_{2z}^{E,H}$ is the wave vector along the propagation direction z inside the material slab; i.e., we have

$$k_{2z}^{E,H} = \frac{\omega}{c}\sqrt{\varepsilon^{E,H}\mu^{E,H} - \sin^2\theta_I}, \tag{A4}$$

where θ_I represents the angle of incidence depicted in Fig. 1. For the parameter χ we have for the case of E waves and $\theta_I \neq 0$,

$$\chi^E = \frac{c}{\mu^E\omega}\frac{k_{2z}^E}{\sqrt{1-\sin^2\theta_I}}, \tag{A5}$$

while for H waves and $\theta_I \neq 0$,

$$\chi^H = \frac{c}{\varepsilon^H\omega}\frac{k_{2z}^H}{\sqrt{1-\sin^2\theta_I}}. \tag{A6}$$

Note that for the simple case of normal incidence, i.e., $\theta_I = 0$, we have that

$$\chi^{E,H} = \sqrt{\frac{\varepsilon^{E,H}}{\mu^{E,H}}}. \tag{A7}$$

Note that we take $\mu^{E,H} = 1$ for purely electric EM response. Also all the above formulas are general and encompass cases with lossy components.

APPENDIX B: DISPERSION RELATIONS FOR EM WAVE PROPAGATION IN A HOMOGENIZED UNIAXIAL METAMATERIAL: EXTRAORDINARY AND ORDINARY WAVES

We assume we have a homogenized 2D composite metamaterial, with purely electric response, following the permittivity tensor given in Eq. (3). Solving Maxwell's equations for such a medium yields two distinct possibilities for the EM wave dispersion relations $\omega(\mathbf{k})$:

$$\varepsilon^H\frac{\omega^2}{c^2} = k_x^2 + k_y^2 + k_{2z}^2, \tag{B1}$$

$$\frac{\omega^2}{c^2} = \frac{k_x^2 + k_{2z}^2}{\varepsilon^E} + \frac{k_y^2}{\varepsilon^H}. \tag{B2}$$

The first branch for the dispersion relation $\omega(\mathbf{k})$, given by Eq. (B1), is normally referred to as the ordinary[7] branch. Conversely, the second branch given by Eq. (B2) is normally referred to as the extraordinary[7] branch. Note that k_x and k_y are the wave vector components that are parallel to the interface, and they are so conserved, i.e.,

$$k_x = \frac{\omega}{c}\sin\psi\cos\phi \tag{B3}$$

and

$$k_y = \frac{\omega}{c}\sin\psi\sin\phi, \tag{B4}$$

where the angles ψ and ϕ are defined in Fig. 7.

Ordinary waves have the wave vector, electric field vector, and magnetic field vector forming an orthonormal set of vectors, while extraordinary[7] waves have wave vector, electric field vector, and magnetic field vector not mutually perpendicular.[7,34,35] These two branches were shown pictorially for a general case in Fig. 8, as surfaces corresponding to a certain frequency, ω.

APPENDIX C: TRANSMISSION THROUGH A HOMOGENEOUS UNIAXIAL SLAB: GENERAL ILLUMINATION CASE

Below we present how to calculate transmission through a homogeneous slab of uniaxial material, with its optical axis along the surface, for an illumination with azimuth $\phi \neq 0$ or 180°. (Such cases were treated in Appendix A). The formulas below apply for a uniaxial slab with electric response only, i.e., $\mu^E = \mu^H = 1$, and encompass cases of lossy materials.

1. Illumination with azimuth $\phi = \pi/2$ or $\phi = 3\pi/2$

In such case we have coupling only to the ordinary branch for S-polarized incident waves or only to the extraordinary branch for P-polarized waves. Then transmission is simply

$$T^{P,S} = \frac{1}{\frac{1}{4}\left|2\cos k_{2z}^{P,S}L - i\left(\chi^{P,S} + \frac{1}{\chi^{P,S}}\right)\sin k_{2z}^{P,S}L\right|^2}, \tag{C1}$$

with $\chi^P = \frac{1}{\varepsilon_E}\frac{k_{2z}^P}{k_{1z}}$, for the case of P polarization, and $\chi^S = \frac{k_{2z}^S}{k_{1z}}$ for the case of S polarization. As before k_{1z} represents the z component of the wave vector of the incoming EM, i.e., $k_{1z} = \frac{\omega}{c}\cos\psi$, with the angle ψ indicated in Fig. 7. We obtain k_{2z}^P from Eq. (B2) for P waves and k_{2z}^S, from Eq. (B1) for S waves. Note that k_x and k_y are the wave vector components conserved parallel to the interface and are equal to 0 and $\frac{\omega}{c}\sin\psi$, respectively.

2. Illumination with arbitrary azimuth: $\phi \neq 0, \pi/2, \pi, 3\pi/2, 2\pi$

For the case of arbitrary azimuth, the propagation inside the uniaxial slab is quite complex. We have simultaneous excitation of both ordinary and extraordinary waves and polarization rotation inside the medium. Normally, such cases were treated with the simple Jones method.[37] However, such method is crude as it neglect reflections from the second interface, which can be particularly important for cases with higher index of refraction. We adopt therefore an exact method, developed by P. Yeh, the 4×4 transfer matrix method.[33] This method is a generalization of the known 2×2 transfer matrix method suitable for homogeneous slabs or multilayers made from isotropic optical media.[36,37]

We solve the system in a new coordinate system $\mathbf{r}' = (x', y', z)$ where $\mathbf{r}' = R(\phi)\mathbf{r}$, with $R(\phi)$ being the rotation matrix[38] for angle ϕ around axis z. Thus in this new coordinate system we have $k_x' = \frac{\omega}{c}\sin\psi$ and $k_y' = 0$. We decompose the electric field outside the slab into its S and P polarization components. Note that in the $\mathbf{r}'$ coordinate system we would have that the electric field for an incident S-polarized wave is parallel to y' and the P-polarized wave lies in the $x'z$ plane. Inside the uniaxial slab the field is decomposed into its normal modes (the ordinary and extraordinary wave). Then continuity of the tangential components of the electric field

E and magnetic field H enable us to relate the incident and scattered S and P polarized fields as follows:

$$\begin{bmatrix} A_S \\ B_S \\ A_P \\ B_P \end{bmatrix} = M_{\text{uni}} \begin{bmatrix} C_S \\ 0 \\ C_P \\ 0 \end{bmatrix}. \tag{C2}$$

A_S, B_S, C_S represent the incident, reflected, and transmitted S-polarized components. Conversely, A_P, B_P, C_P represent the incident, reflected, and transmitted P-polarized components. The 4×4 uniaxial medium transfer matrix M_{uni} has the following form:[33]

$$M_{\text{uni}} = D_{\text{air}}^{-1} D_{\text{slab}} P(L) D_{\text{slab}}^{-1} D_{\text{air}}. \tag{C3}$$

In Eq. (C3) D_{air} and D_{slab} are the dynamical matrices[33,39] for air and the uniaxial medium, and $P(L)$ is the propagation matrix through the uniaxial slab of thickness L. These are given by the following expressions:

$$D_{\text{air}} = \begin{bmatrix} \hat{x}' \cdot \hat{p}_S^+ & \hat{x}' \cdot \hat{p}_S^- & \hat{x}' \cdot \hat{p}_P^+ & \hat{x}' \cdot \hat{p}_P^- \\ \hat{y}' \cdot \hat{q}_S^+ & \hat{y}' \cdot \hat{q}_S^- & \hat{y}' \cdot \hat{q}_P^+ & \hat{y}' \cdot \hat{q}_P^- \\ \hat{y}' \cdot \hat{p}_S^+ & \hat{y}' \cdot \hat{p}_S^- & \hat{y}' \cdot \hat{p}_P^+ & \hat{y}' \cdot \hat{p}_P^- \\ \hat{x}' \cdot \hat{q}_S^+ & \hat{x}' \cdot \hat{q}_S^- & \hat{x}' \cdot \hat{q}_P^+ & \hat{x}' \cdot \hat{q}_P^- \end{bmatrix}, \tag{C4}$$

$$D_{\text{slab}} = \begin{bmatrix} \hat{x}' \cdot \hat{p}_{EO}^+ & \hat{x}' \cdot \hat{p}_{EO}^- & \hat{x}' \cdot \hat{p}_O^+ & \hat{x}' \cdot \hat{p}_O^- \\ \hat{y}' \cdot \hat{q}_{EO}^+ & \hat{y}' \cdot \hat{q}_{EO}^- & \hat{y}' \cdot \hat{q}_O^+ & \hat{y}' \cdot \hat{q}_O^- \\ \hat{y}' \cdot \hat{p}_{EO}^+ & \hat{y}' \cdot \hat{p}_{EO}^- & \hat{y}' \cdot \hat{p}_O^+ & \hat{y}' \cdot \hat{p}_O^- \\ \hat{x}' \cdot \hat{q}_{EO}^+ & \hat{x}' \cdot \hat{q}_{EO}^- & \hat{x}' \cdot \hat{q}_O^+ & \hat{x}' \cdot \hat{q}_O^- \end{bmatrix}, \tag{C5}$$

$$P(L) = \begin{bmatrix} e^{-ik_{EO}L} & 0 & 0 & 0 \\ 0 & e^{ik_{EO}L} & 0 & 0 \\ 0 & 0 & e^{-ik_O L} & 0 \\ 0 & 0 & 0 & e^{ik_O L} \end{bmatrix}. \tag{C6}$$

In the above expressions $\hat{p}_S$, $\hat{p}_P$ are normalized vectors indicating the direction of the electric field for an S-polarized wave and a P-polarized wave, respectively, in the air medium. On the other hand, $\hat{p}_{EO}$, $\hat{p}_O$ are normalized vectors representing the direction of the electric field inside the uniaxial medium for the extraordinary and the ordinary wave, respectively. p vectors with the $+$ superscript correspond to waves traveling downward (see schematics of Fig. 7) while p vectors with the $-$ superscript correspond waves to traveling upward. Note that $\hat{x}'$, $\hat{y}'$ are the unit vectors along the surface in the rotated $x'y'z$ system. Thus we have

$$\hat{p}_S^+ = \hat{p}_S^- = \hat{y}', \tag{C7}$$

$$\hat{p}_P^+ = -\cos\psi \hat{x}' + \sin\psi \hat{z}, \tag{C8}$$

$$\hat{p}_P^- = -\cos\psi \hat{x}' - \sin\psi \hat{z}, \tag{C9}$$

$$\hat{p}_{EO}^+ = \frac{1}{N_{EO}}(p_{EO,x'}^+ \hat{x}' + p_{EO,y'}^+ \hat{y}' + \hat{z}), \tag{C10}$$

$$\hat{p}_{EO}^- = \frac{1}{N_{EO}}(-p_{EO,x'}^+ \hat{x}' - p_{EO,y'}^+ \hat{y}' + \hat{z}), \tag{C11}$$

where

$$p_{EO,x'}^+ = \frac{k_x}{k_{EO}}\cos\phi - \frac{k_x^2 + k_{EO}^2}{k_{EO}k_y}\frac{\varepsilon^H}{\varepsilon^E}\sin\phi, \tag{C12}$$

$$p_{EO,y'}^+ = -\frac{k_x}{k_{EO}}\sin\phi - \frac{k_x^2 + k_{EO}^2}{k_{EO}k_y}\frac{\varepsilon^H}{\varepsilon^E}\cos\phi, \tag{C13}$$

and

$$N_{EO} = \sqrt{|p_{EO,x'}^+|^2 + |p_{EO,y'}^+|^2 + 1}. \tag{C14}$$

Now for the direction of the electric field of the ordinary wave we have

$$\hat{p}_O^+ = \frac{1}{N_O}(p_{O,x'}^+ \hat{x}' + p_{O,y'}^+ \hat{y}' + \hat{z}) \tag{C15}$$

and

$$\hat{p}_O^- = \frac{1}{N_O}(-p_{O,x'}^+ \hat{x}' - p_{O,y'}^+ \hat{y}' + \hat{z}), \tag{C16}$$

where

$$p_{O,x'}^+ = -\frac{k_O}{k_x}\cos\phi, \tag{C17}$$

$$p_{O,y'}^+ = \frac{k_O}{k_x}\sin\phi, \tag{C18}$$

and

$$N_O = \sqrt{|p_{O,x'}^+|^2 + |p_{O,y'}^+|^2 + 1}. \tag{C19}$$

In Eqs. (C7) through (C18), the angles ϕ and ψ are defined in Fig. 7, and k_x, k_y are the components of the incident wave vector parallel to the interface that are conserved through the entire structure, given by the expressions in Eqs. (B3) and (B4), respectively. Now, k_{EO} and k_O are the wave vector components along z, k_{2z} corresponding to the extraordinary and ordinary branch, respectively, as expressed in Eqs. (B2) and (B1).

The $\hat{q}$ give the directions of the respective magnetic fields; i.e., (since all media are nonmagnetic)

$$\hat{q} = \left(\sin\psi \hat{x}' + \frac{ck_{2z}}{\omega}\hat{z}\right) \times \hat{p}, \tag{C20}$$

where we would substitute the respective $\hat{p}$ vectors and k_{2z} for each case.

Equations (C3) through (C20) together with Eqs. (B1)–(B4) provide all the necessary information to calculate numerically the 4×4 transfer matrix M_{uni}. Then the transmission for the case of S-polarized waves would be[33]

$$T = |t_{ss}|^2 + |t_{sp}|^2 \tag{C21}$$

and for the case of P polarization

$$T = |t_{pp}|^2 + |t_{ps}|^2, \tag{C22}$$

where,

$$t_{ss} = \frac{M_{\text{uni},33}}{M_{\text{uni},11}M_{\text{uni},33} - M_{\text{uni},13}M_{\text{uni},31}}, \tag{C23}$$

$$t_{sp} = \frac{-M_{\text{uni},31}}{M_{\text{uni},11}M_{\text{uni},33} - M_{\text{uni},13}M_{\text{uni},31}}, \tag{C24}$$

$$t_{ps} = \frac{-M_{\text{uni},13}}{M_{\text{uni},11}M_{\text{uni},33} - M_{\text{uni},13}M_{\text{uni},31}}, \tag{C25}$$

$$t_{pp} = \frac{M_{\text{uni},11}}{M_{\text{uni},11}M_{\text{uni},33} - M_{\text{uni},13}M_{\text{uni},31}}. \tag{C26}$$

Note that the factors t_{sp} and t_{ps} represent cross-polarization terms which are nonzero.

APPENDIX D: RETRIEVAL OF THE EM CONSTITUTIVE PARAMETERS IN UNIAXIAL METAMATERIAL COMPOSITES

The reflectivity over transmissivity through a homogeneous uniaxial material slab is given from Eq. (A3). For the specific case of normal incidence along the z direction (see Fig. 1), for which we perform the retrieval process, and for the general case with magnetic behavior present, the χ parameter for E and H waves would be given by Eq. (A7), with $k_{2z}^{E,H}$ given by

$$k_{2z}^{E,H} = n^{E,H}\frac{\omega}{c}, \tag{D1}$$

with

$$n^{E,H} = \sqrt{\varepsilon^{E,H}\mu^{E,H}}, \tag{D2}$$

where the superscripts E, H apply for the case of E waves and H waves, respectively.

We have assumed a uniaxial metamaterial with permittivity and permeability tensors given by Eqs. (3) and (4), respectively. Equation (A3) yields

$$n^{E,H} = \frac{c}{\omega L}\left(\cos^{-1}\frac{\left(\frac{r}{t}\right)_{2L}}{2\left(\frac{r}{t}\right)_{L}} + l\pi\right). \tag{D3}$$

In the above equation $\cos^{-1}$ represents the principal value of the function and l the order of the branch. Since the solution we obtain for the refractive index $n^{E,H}$ is multibranched, we need to have data for a few thicknesses L to identify which branch yields the correct solution. Once we have the refractive index $n^{E,H}$, we can obtain $\chi^{E,H}$ from the following equation:

$$\chi^{E,H} - \frac{1}{\chi^{E,H}} = \frac{\left(\frac{r}{t}\right)_{L}}{\frac{i}{2}\sin(n^{E,H}\frac{\omega L}{c})}. \tag{D4}$$

The above equation provides two solutions for $\chi^{E,H}$, from which we chose the one with $\text{Re}(\chi^{E,H}) > 0$, which is appropriate for passive materials (Refs. 42,43). Now knowing $n^{E,H}$ and $\chi^{E,H}$, we can obtain the effective permittivities for both E waves and H waves, ε^{E} and ε^{H}, and corresponding effective permeabilities, μ^{E} and μ^{H}, from the following equations:

$$\varepsilon^{E,H} = n^{E,H}\chi^{E,H} \tag{D5}$$

and

$$\mu^{E,H} = \frac{n^{E,H}}{\chi^{E,H}}. \tag{D6}$$

[1] B. Ferguson and X.-C. Zhang, Nature Mater. **1**, 26 (2002).
[2] J. Faist, F. Capasso, D. L. Sivco, C. Sirtori, A. L. Hutchinson, and A. Y. Cho, Science **264**, 553 (1994).
[3] R. Kohler, A. Tredicucci, F. Betram, H. E. Beere, E. H. Linfield, A. G. Davies, D. A. Ritchie, R. C. Iotti, and F. Rossi, Nature (London) **417**, 156 (2002).
[4] C. Gmachl, F. Capasso, D. L. Sivco, and A. Y. Cho, Rep. Prog. Phys. **64**, 1533 (2001).
[5] Y. M. Liu, G. Bartal, and X. Zhang, Opt. Express **16**, 15439 (2008).
[6] A. Fang, T. Koschny, and C. M. Soukoulis, Phys. Rev. B **79**, 245127 (2009).
[7] M. Born and E. Wolf, *Principles of Optics : Electromagnetic Theory of Propagation, Interference, and Diffraction of Light* (Pergamon Press, 1980).
[8] S. Foteinopoulou and C. M. Soukoulis, Phys. Rev. B **72**, 165112 (2005).
[9] D. R. Smith and D. Schurig, Phys. Rev. Lett. **90**, 077405 (2003).
[10] M. C. K. Wiltshire, J. B. Pendry, I. R. Young, D. J. Larkman, D. J. Gilderdale, and J. V. Hajnal, Science **291**, 849 (2001).
[11] A. Salandrino and N. Engheta, Phys. Rev. B **74**, 075103 (2006).
[12] D. Schurig and D. R. Smith, New J. Phys. **7**, 162 (2005).
[13] K. C. Huang, P. Bienstman, J. D. Joannopoulos, K. A. Nelson, and S. H. Fan, Phys. Rev. Lett. **90**, 196402 (2003).
[14] D. A. G. Bruggeman, Ann. Phys. (Leipzig) **24**, 636 (1935).
[15] J. C. M. Garnett, Philos. Trans. R. Soc. London A **203**, 385 (1904); **205**, 237 (1906).
[16] A. Kirchner, K. Busch, and C. M. Soukoulis, Phys. Rev. B **57**, 277 (1998).
[17] V. Yannopapas, A. Modinos, and N. Stefanou, Phys. Rev. B **60**, 5359 (1999).
[18] K. Busch and C. M. Soukoulis, Phys. Rev. B **54**, 893 (1996).
[19] A. A. Krokhin, P. Halevi, and J. Arriaga, Phys. Rev. B **65**, 115208 (2002).

[20]J. Elser, R. Wangberg, V. A. Podolskiy, and E. E. Narimanov, Appl. Phys. Lett. **89**, 261102 (2006).

[21]C. A. Kyriazidou, H. E. Contopanagos, W. M. Merill, and N. G. Alexopoulos, IEEE Trans. Antennas Propag. **48**, 95 (2000).

[22]V. Yannopapas, Phys. Rev. B **75**, 035112 (2007).

[23]More commonly in optics E polarization and H polarization are known as TE and TH polarization, respectively. The reason we use the former is to be consistent also with PC terminology. In the place of the slabs seen in Fig. 1, representing the homogenized medium seen, we will consider a 2D PC medium with rods along y and the plane of periodicity on the xz plane.

[24]J. D. Joannopoulos, S. G. Johnson, J. N. Winn, and R. D. Meade, *Photonic Crystals: Molding the Flow of Light*, Second Edition (Princeton University Press, 2008).

[25]K. M. Ho, C. T. Chan, and C. M. Soukoulis, Phys. Rev. Lett. **65**, 3152 (1990).

[26]P. M. Bell, J. B. Pendry, L. M. Moreno, and A. J. Ward, Comput. Phys. Commun. **182**, 306 (1995).

[27]We note that points with small magnitude of $|r/t|$ contribute unavoidably very large error in the numerical evaluation of η, or $B(\theta_I)$, and are thus excluded.

[28]We exclude in the average point $L = 1a$, where bulk properties of the medium would not apply.

[29]Evidently, the total number of different thickness values between $L = 1a$ and $L = 30a$ participating in the average can be less than 30. We do not plot frequencies for which we could not obtain at least 10 participating thickness values.

[30]S. Foteinopoulou, A. Rosenberg, M. M. Sigalas, and C. M. Soukoulis, J. Appl. Phys. **89**, 824 (2001).

[31]J. A. Kong, *Electromagnetic Wave Theory* (John Wiley and Sons, 1986).

[32]P. St. J. Russell, T. A. Birks, and F. Dominic Lloyd-Lucas, in *Confined Electrons and Photons, New Physics and Applications*, Vol. 340 of NATO Advanced Studies Institute, Series B: Physics, edited by E. Burstein and C. Weisbuch (Plenum, New York, 1995), p. 585.

[33]P. Yeh, J. Opt. Soc. Am. **69**, 742 (1979).

[34]I. V. Lindell, S. A. Tretyakov, K. I. Nikoskinen, and S. Ilvonen, Microwave Opt. Tech. **31**, 129 (2001).

[35]N. H. Shen, S. Foteinopoulou, M. Kafesaki, T. Koschny, E. Ozbay, E. N. Economou, and C. M. Soukoulis, Phys. Rev. B **80**, 115123 (2009).

[36]P. Markos and C. M. Soukoulis, *Wave Propagation: From Electrons to Photonic Crystals and Left-Handed Materials* (Princeton University Press, 2008).

[37]A. Yariv and P. Yeh, *Optical Waves in Crystals* (John Wiley and Sons, 1984).

[38]G. Arfken, *Mathematical Methods for Physicists* (Academic Press, Inc., 1985).

[39]C. Vandenbem, J. P. Vigneron, and J. M. Vigoureux, J. Opt. Soc. Am. B **23**, 2366 (2006).

[40]E. D. Palik, *Handbook of Optical Constants of Solids* (Academic Press, 1985).

[41]Eq. (10) represents the proper Lorentzian form of the permittivity with $\Gamma > 0$ for waves of the form $e^{i\mathbf{k}\cdot\mathbf{r}}e^{-i\omega t}$ (physics convention).

[42]D. R. Smith, S. Schultz, P. Markos, and C. M. Soukoulis, Phys. Rev. B **65**, 195104 (2002).

[43]D. R. Smith, D. C. Vier, T. Koschny, and C. M. Soukoulis, Phys. Rev. E **71**, 036617 (2005).

[44]J. F. Zhou, T. Koschny, M. Kafesaki, and C. M. Soukoulis, Phys. Rev. B **80**, 035109 (2009).

[45]For the polaritonic PC, the band structure was calculated with a plane wave method adapted to treat dispersive media as in Ref. 46.

[46]C. S. Feng, L. M. Mei, L. Z. Cai, X. L. Yang, S. S. Wei, and P. Li, J. Phys. D **39**, 4316 (2006).

[47]K. C. Huang, M. L. Povinelli, and J. D. Joannopoulos, Appl. Phys. Lett. **85**, 543 (2004).

[48]K. Vynck, D. Felbacq, E. Centeno, A. I. Cabuz, D. Cassagne, and B. Guizal, Phys. Rev. Lett. **102**, 133901 (2009).

[49]W. Cai and V. Shalaev, *Optical Metamaterials: Fundamentals and Applications* (Springer, 2010).

[50]T. Koschny, P. Markos, D. R. Smith, and C. M. Soukoulis, Phys. Rev. E **68**, 065602(R) (2003).

[51]C. M. Soukoulis, S. Linden, and M. Wegener, Science **315**, 47 (2007).

[52]J. Valentine, S. Zhang, T. Zentgraf, E. Ulin-Avila, D. A. Genov, G. Bartal, and X. Zhang, Nature (London) **455**, 376 (2008).

[53]E. N. Economou, M. Kafesaki, C. M. Soukoulis, and T. Koschny, J. Comp. Theor. Nanoscience **6**, 1827 (2009).

[54]A. J. Hoffman, L. Alekseyev, S. S. Howard, K. J. Franz, D. Wasserman, V. A. Podolskiy, E. E. Narimanov, D. L. Sivco, and C. Gmachl, Nature Mater. **6**, 946 (2007).

[55]C. E. Krieger, M. S. Rill, S. Linden, and M. Wegener, IEEE J. Sel. Top. Quantum Electron. **16**, 367 (2010).